

1 **Influence of bank slope on sinuosity-driven hyporheic exchange flow and**  
2 **residence time distribution during a dynamic flood event**

3

4 **Manuscript submitted to Hydrology and Earth System Sciences**

5

6 Yiming Li<sup>1,2</sup>, Uwe Schneidewind<sup>2</sup>, Zhang Wen<sup>1\*</sup>, Stefan Krause<sup>2</sup>, Hui Liu<sup>1</sup>

7

8 <sup>1</sup>Hubei Key Laboratory of Yangtze River Catchment Environmental Aquatic Science,  
9 School of Environmental Studies, China University of Geosciences, People's Republic  
10 of China

11 <sup>2</sup>School of Geography, Earth and Environmental Sciences, University of Birmingham,  
12 UK

13

14 **\*Correspondence:** Zhang Wen (wenz@cug.edu.cn)

---

15 **Abstract.** This study uses a reduced-order two-dimensional (2-D) horizontal model to  
16 investigate the influence of riverbank slope on the sinuosity-driven hyporheic exchange  
17 process along sloping alluvial riverbanks during a transient flood event. The Deformed  
18 Geometry Method (DGM) is applied to quantify the displacement of the sediment-  
19 water interface (SWI) along the sloping riverbank during river stage fluctuation. This  
20 new modeling approach serves as the initial step focusing on the impact of bank slope  
21 on the hyporheic exchange flux (HEF) and the residence time distribution (RTD) of  
22 pore water in the fluvial aquifer for a sinuosity-driven river corridor. Several controlling  
23 factors, including sinuosity, alluvial valley slope, river flow advective forcing and  
24 duration of flow are incorporated into the model to investigate the effects of bank slope  
25 on aquifers of variable hydraulic transmissivity. Compared to simulations of a vertical  
26 riverbank, sloping riverbanks were found to increase the HEF. For sloping riverbanks,  
27 the hyporheic zone (HZ) encompasses a larger area and penetrated deeper into the  
28 alluvial aquifer, especially in aquifers with smaller transmissivity (i.e., due to increased  
29 hydraulic conductivity or reduced specific yield). Furthermore, consideration of sloping  
30 banks as compared to a vertical river bank can lead to both underestimation or  
31 overestimation of the pore water travel time. The impact of bank slope on residence  
32 time was more pronounced during a flood event for high transmissivity aquifer  
33 conditions, while it had a long-lasting influence after the flood event in lower  
34 transmissivity aquifers. Consequently, ~~this~~ [the impact of bank slope](#) decreases the travel  
35 time of water discharging into the river relative to base flow conditions. These findings  
36 highlight the need for (re)consideration of the importance of ~~more~~ complex riverbank  
37 morphology [conceptualization in numerical models as control of hyporheic exchange](#)  
38 [in floodplains when account for the HEF and RTD](#). The results have potential  
39 implications for river management and restoration and the management of river and  
40 groundwater pollution.

41

42 **Key words:** hyporheic exchange, sloping riverbank, deformed geometry, numerical

---

43 simulation, residence time distribution

## Nomenclature

$\Delta L$	Nodal spacing [m]
$\nabla$	Laplace operator
$\alpha_L$	Longitudinal dispersivity [L]
$\alpha_T$	Transverse dispersivity [L]
<b>D</b>	Dispersion-diffusion tensor [ $L^2T^{-1}$ ]
$D_L$	Water diffusivity [ $L^2T^{-1}$ ]
$J_x$	Base groundwater gradient [-]
$K$	Hydraulic conductivity [ $LT^{-1}$ ]
$n$	Scaling number [-]
$n_0$	Intensity of flood event [-]
$n_d$	Skewness of flood event [-]
$S_y$	Specific yield [-]
$t_d$	Duration of flood event [T]
$t_p$	Time to peak river stage [T]
$\alpha$	Amplitude of the river boundary [L]
$\Gamma_d$	Dimensionless aquifer transmissivity [-]
$\delta$	Bank slope angle [ $^\circ$ ]
$\delta_{ij}$	Kronecker delta function [-]
$\epsilon$	Tortuosity [-]
$\eta$	Degree of flood event asymmetry [ $T^{-1}$ ]
$\theta$	Effective porosity [-]
$\lambda$	River boundary wave length [L]
$\sigma$	River boundary sinuosity [-]
$\tau$	Residence time [T]
$\omega$	Flood event frequency [ $T^{-1}$ ]
$h(\mathbf{x}, t)$	Transient groundwater head [L]
$\Delta h^*$	Dimensionless parameter of ambient groundwater flow [-]

$A^{**}(t)$	Dimensionless variation of HZ area relative to base flow conditions [-]
$C(\mathbf{x}, t)$	Solute concentration in the aquifer [ $\text{ML}^{-3}$ ]
$C_0(\mathbf{x})$	Solute concentration as initial condition [ $\text{ML}^{-3}$ ]
$C_S(\mathbf{x}, t)$	Solute concentration in the river [ $\text{ML}^{-3}$ ]
$d^{**}(t)$	Dimensionless variation of HZ penetration distance relative to base flow conditions [-]
$H(\mathbf{x}, t)$	Thickness of the saturated aquifer [L]
$H_0(\mathbf{x})$	Initial river stage [L]
$H_p$	Peak river stage during the flood event [L]
$H_r(t)$	River stage at the downstream end [L]
$h_r(x, t)$	Transient river stage [L]
$M(t)$	Displacement of the sediment-water interface [L]
$P_e$	Péclet number [-]
$\mathbf{q}$	Specific discharge or Darcy flux [ $\text{LT}^{-1}$ ]
$\mathbf{Q}$	Aquifer-integrated discharge [ $\text{L}^2\text{T}^{-1}$ ]
$Q_{in, HZ}^*(t)$	Dimensionless net flux along the river boundary [-]
$Q_{in, HZ}^*(t)$	Dimensionless exchange flux from the aquifer to the river [-]
$Q_{out, HZ}^*(t)$	Dimensionless exchange flux from the river to the aquifer [-]
$Y(x, t)$	Location of the sediment-water interface boundary [L]
$z_b(\mathbf{x})$	Elevation of the underlying impermeable layer [L]
$\Gamma_d$	Dimensionless parameter of aquifer transmissivity [-]
$\mu_r(\mathbf{x}, 0)$	Mean (first order of) residence time distribution [T]
$\mu_{out}^*(x, t)$	Flux-weighted ratio of mean RT to mean RT under baseflow conditions [-]
$\mu_n(\mathbf{x}, t)$	$n$ -th moment of residence time distribution [ $\text{T}^n$ ]
$\mu_r^*(\mathbf{x}, t)$	<a href="#">Mean r</a> Residence time distribution ratio between slope and vertical river bank model [-]
$\mu_{\tau 0-\max}$	Maximum RT in the domain [T]

$\mu_{\tau-S}(\mathbf{x}, t)$	<a href="#">Mean r</a> Residence time distribution of slope river bank model [T]
$\mu_{\tau-V}(\mathbf{x}, 0)$	<a href="#">Mean r</a> Residence time distribution of vertical river bank model [T]
$\rho(\mathbf{x}, t, \tau)$	Residence time distribution [T]

### Abbreviations

HZ	Hyporheic zone
HEF	Hyporheic exchange flux
DGM	Deformed Geometry Method
SWI	Sediment-water interface
RTD	Residence time distribution
RT	Residence time
ALE	Arbitrary Lagrangian–Eulerian
2-D	Two-dimensional
BTS	Biogeochemical timescale

44

45

---

## 46 1. Introduction

47 The hyporheic zone (HZ) can be described as the region that connects the river  
48 channel and adjacent aquifer, and includes riverbed and riverbanks. Mixing and  
49 transporting of different water types (groundwater, surface water) and [water](#) ages in the  
50 HZ driven by hydrodynamic and hydrostatic factors cause spatially and temporally  
51 varying exchange of water and biogeochemical species between river channel, riverbed  
52 and aquifer (Cardenas, 2009b; Hester and Gooseff, 2010; Krause et al., 2011, 2017,  
53 2022; McClain et al., 2013; Boano et al., 2014). The hyporheic exchange flux (HEF)  
54 represents the interaction flux between surface water and groundwater in vertical (e.g.,  
55 bedform-driven) and horizontal/[lateral](#) (e.g., meander-driven) directions, which can add  
56 to general regional groundwater ex-filtration and infiltration. The distribution of  
57 hyporheic flow paths strongly determines the spatial and temporal distribution of  
58 hydrogeochemical characteristics of water within the riverbed and the wider river  
59 corridor as well as the formation of so-called hot zones and hot moments (Krause et al.,  
60 2013, 2017; Cardenas, 2015; Pinay et al., 2015).

61 ~~Hyperheic exchange flux~~ (HEF) is controlled by parameters such as stream  
62 discharge dynamics, recharge, riverbed and aquifer hydraulic properties, local  
63 hydraulic head fluctuations, as well as river geometry and morphology including  
64 sinuosity and riverbank slope (Larkin and Sharp, 1992; Gomez-Velez et al., 2012; 2017;  
65 Schmadel et al., 2016). For example, Cardenas et al. (2004) demonstrated how riverbed  
66 characteristics and especially the heterogeneity of hydraulic conductivity could  
67 increase HEF by 17% to 32%. As such, ~~to be able to better~~ [a better](#) estimateion of the  
68 relative importance of HEF on catchment water fluxes and biogeochemical processes  
69 requires a good understanding of its different drivers and controls. This is imperative  
70 as the spatiotemporal ~~progression evolution~~ of HEF, the resulting change in HZ (area)  
71 and thus also the residence or travel time (RT) of the exchanged water in the HZ have  
72 significant impact on flow dynamics and transient storage along the river continuum

---

73 and in turn control the capacity for contaminant attenuation (Weatherill et al., 2018)  
74 and biogeochemical functions of river corridors (Bertrand et al., 2012; Boulton et al.,  
75 2010; Brunke and Gonser, 1997).

76 Both lateral exchange between river and its floodplain, as well as bedform-  
77 induced vertical exchange at the streambed interface have been found to be crucial with  
78 regards to HEF and the biogeochemical transformation potential along the river corridor  
79 (Boano et al., 2010, 2014; Gomez-Velez and Harvey, 2014; Gomez-Velez et al., 2015,  
80 2017; Kiel and Cardenas, 2014; Stonedahl et al., 2013). ~~Through~~ By using numerical  
81 simulations, considerable progress has been made with regards to our understanding of  
82 how river planform geometry (Boano et al., 2006, 2010; Cardenas 2006; 2008; 2009a,  
83 2009b; Stonedahl 2013), dynamic flood events (Gomez-Velez et al., 2012; 2017) and  
84 evapotranspiration (Kruegler et al., 2020) control HEF. Focusing on lateral exchange  
85 flow processes, Cardenas (2008; 2009a, 2009b) utilized numerical models to  
86 investigate HEF and residence time distribution (RTD) for various river channel  
87 morphologies and regional groundwater flow conditions. Their simulations indicate  
88 that channel morphology, represented by sinuosity, is a dominant factor controlling HEF,  
89 the total HZ area, and RTD. In addition, Boano et al. (2010) used a similar modeling  
90 framework to study the relationship between RTD and biogeochemical transformation  
91 by introducing surface water as a major source of dissolved organic matter that triggers  
92 a sequence of redox reactions within the HZ. Reactive transport simulations showed a  
93 good relationship between RTD and denitrification reaction potential. Based on these  
94 studies, Gomez-Velez et al. (2012) conducted numerical simulations to investigate the  
95 impact of aquifer parameters (water table gradient, hydraulic conductivity, dispersivity)  
96 and channel sinuosity on HEF and RTD. The authors analyzed the RTD underfor  
97 various aquifer conditions to study ~~classify whether~~ when a meander can play a role as  
98 boths as a source or sink of nitrate. ~~By comparing RTD with the timescale of~~  
99 ~~nitrification/denitrification reactions, a meander can be classified as a source or sink of~~  
100 ~~nitrate.~~ More recent modeling studies focused predominantly on the effects of dynamic



101 river/groundwater stage fluctuations on lateral (e.g., Schmadel et al., 2016; Gomez-  
102 Velez et al., 2017) and vertical (e.g., Singh et al., 2019, 2020; Wu et al., 2018, 2020,  
103 2021) hyporheic exchange and RTD. For example, Gomez-Velez et al. (2017) explored  
104 the HZ response to a dynamic river stage due to variable hydraulic conductivity,  
105 groundwater flow gradient and river sinuosity conditions. Their results indicate that  
106 ~~during a flood event~~ the dynamic forcing greatly influences net HEF, the area of ~~the~~ HZ  
107 ~~as well as mean~~ ~~nd~~-RTD across different ~~setting~~~~scenarios~~, whereby ~~the aquifer~~  
108 ~~transmissivity is one of the key parameters. determines the magnitude and lasting time~~  
109 ~~of HEF and RTD to a flood event. higher aquifer transmissivity will likely result in a~~  
110 ~~stronger but shorter response of HEF and RTD to a flood event.~~

111 Although there is a considerable body of numerical research on the lateral  
112 hyporheic response to the various geometrical (e.g., geometry of river channel, river  
113 slope, etc) and dynamic drivers (e.g., fluctuation of river/groundwater, gaining and  
114 losing ~~conditions of groundwater~~~~stream conditions~~, etc.), many HZ studies do not  
115 specifically consider floodplain-driven processes or they ~~apply~~ ~~assume~~ vertical  
116 riverbanks with straight river planimetry in an attempt to reduce model complexity in  
117 line with the analytical or numerical solutions used (Cooper and Rorabaugh, 1963; Hunt,  
118 1990; Schmadel et al., 2016; Gomez-Velez et al., 2017;). However, riverbanks are  
119 usually sloping (inclined) rather than vertical (Liang et al., 2018) as they undergo  
120 erosion ~~(by surface and subsurface water) and gravity collapse~~ (Osma and Thorne, 1988;  
121 ~~Fox and Wilson, 2010~~). Previous research has proven that bank erosion and bank  
122 collapse are ~~globally spreading processes~~ controlled by various factors, such as initial  
123 bank slope angle (Zingg, 1940; Lindow et al., 2009), surface flow forces (Hagerty et  
124 al., 1995; Fox and Wilson, 2010), vegetation cover (Mayor et al., 2008; Gao et al., 2009;  
125 Puttock et al., 2013) and sediment properties (Millar and Quich, 1993). ~~Previous studies~~  
126 ~~have provedemonstrated that n~~Neglecting bank slope ~~when modelling in analytical~~  
127 ~~and numerical river-bank hyporheic exchange model solutions~~ may ~~therefore~~ have a  
128 significant ~~impact influence~~ on ~~the model~~ prediction accuracy ~~of HEF~~ (Doble et al.

129 2012a, 2012b; [Liang et al. 2020](#)) and RTD (Derx et al., 2014; Siergieiev et al., 2015) in  
130 an unconfined floodplain aquifer. Thus, a detailed analysis of the floodplain drivers of  
131 HEF should require a more detailed consideration of the floodplain geometry including  
132 riverbank slope in bank storage conceptual models (Sharp, 1977).

133 A few previous studies have used numerical modeling where the model is bounded  
134 by a sloping riverbank to assess the influence of bank slope on HEF for a vertical section  
135 of an alluvial aquifer. In such cases, the aquifer was considered variably saturated,  
136 homogenous, and isotropic, while flow in the unsaturated zone was calculated using the  
137 Richards equation (Li et al., 2008; McCallum et al., 2010; Doble 2012a; b). These  
138 studies have confirmed that neglecting bank slope can lead to an underestimation of the  
139 bank storage volume as well as the temporal HEF in vertical cross-sectional profiles,  
140 especially under relatively small bank angles.

141 In turn, river sinuosity and ambient groundwater gradient (along the river channel)  
142 have not been studied as potential drivers of sinuosity-driven lateral HEF and RTD and  
143 their biogeochemical implications when a sloping river bank exists and it needs to be  
144 determined whether considering both drivers can lead to significantly different findings  
145 as compared to previous cross-sectional profile models (Doble et al., 2012; Siergieiev  
146 et al., 2015; Derx et al., 2014). In this study, we therefore quantify the effect of bank  
147 slope on the spatial extent (area) of the HZ in sinuosity-driven river meanders [in](#)  
148 [response to a flood event](#) and how it impacts the [progression evolution](#) of HEF and RTD  
149 under varying aquifer transmissivity conditions to better understand lateral HEF  
150 through the alluvial plain. [The RTD represents the distribution of average pore water](#)  
151 [travel time since the infiltration of river water into the system for a given time \(Gomez-](#)  
152 [Velez et al., 2012; Singh et al., 2019\)](#). We build on the numerical modeling approach  
153 introduced by Gomez-Velez et al. (2017) and consider lateral bank slope by coupling  
154 the deformed geometry method (DGM) to the flow (Liang et al. 2020), the solute  
155 transport and the residence time distribution equation. Our results reveal how and when  
156 bank slope plays an important role in sinuosity-driven meandering rivers with respect

---

157 to HEF and RTD, which in turn will lead to an improved understanding of the river  
158 channel-aquifer-floodplain system and provide guidance on the placement of  
159 monitoring locations in river management studies.

160

---

## 161 2. Methodology

### 162 2.1 Model setup using deformed geometry method

163 The modeling approach and dimensionless parameterization ~~metrics~~ used by  
164 Gomez-Velez et al. (2017) can represent most riverbank-aquifer situations and dynamic  
165 flood conditions. In our study, we use their conceptual model to set up a baseline case  
166 with the same model frame, equations and parameterization metrics. Additional  
167 information regarding the implementation of this baseline case can be found in the SI.  
168 However, where their previous research assumed a vertical river bank for sinuosity-  
169 driven HEF ~~models~~, we consider a sloping riverbank and use the [Deformed Geometry](#)  
170 [Method](#) (DGM) approach to capture the dynamic [progression evolution](#) of the [surface](#)  
171 [water interface](#) (SWI) along the river course. A constant sloping angle ( $\delta$  [°]) along the  
172 alluvial riverbank of a sinusoidal river was implemented in our model (see blue lines  
173 of conceptual model in Figure S1 and the corresponding mathematical model in Figure  
174 S2a) while the ~~surface water interface~~ (SWI) was assumed to be always vertical  
175 (vertical solid red and green lines in Figure S2c). As such, the contraction or expansion  
176 of the simulated domain, i.e., displacement of the SWI can be characterized by the  
177 sloping angle (there is no movement of the SWI for the vertical riverbank case) and  
178 river stage. As the river stage changes, so does the location of the SWI.

179 When the river stage changes in our model, the sinusoidal boundary will migrate  
180 towards or away from the floodplain meaning that the submerged part of the riverbank  
181 is considered contracted and our model only considers the alluvial aquifer that is not  
182 submerged. The [evolution changes](#) of the SWI during a flood event can be calculated  
183 by considering river stage and bank slope via:

$$184 \quad Y(x, t) = Y_0(x) + M(t) \quad (1)$$

185 where  $Y(x, t)$  [L] is the location of the SWI boundary while  $Y_0(x)$  [L] is the initial

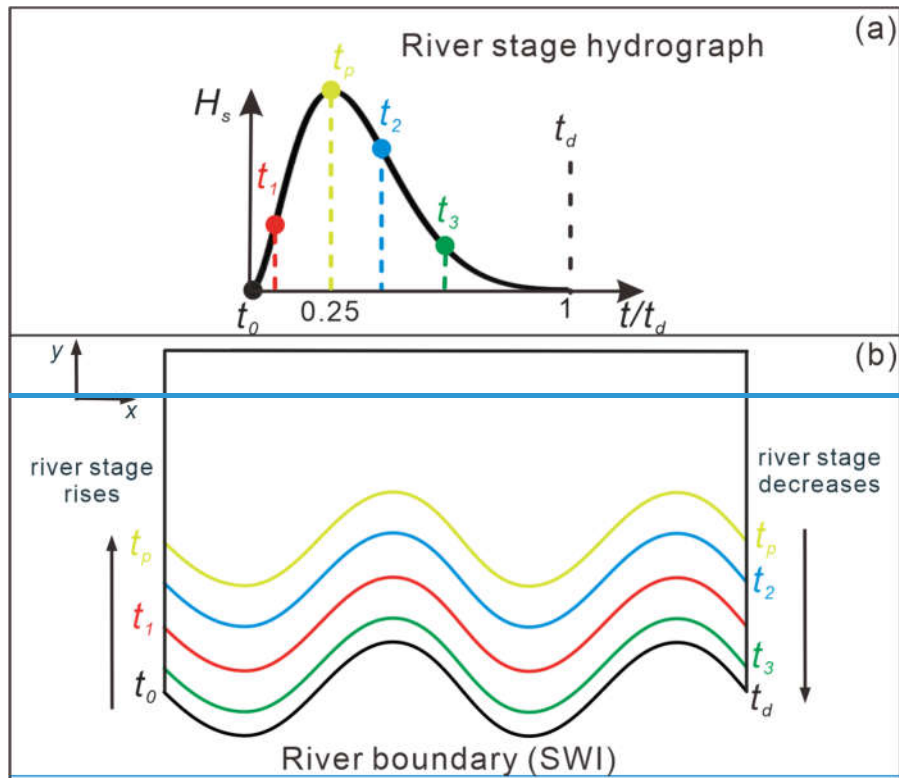
186 location of the SWI.  $M(t) = [h(t) - h(0)]/\tan(\delta)$  is the displacement of the SWI in  $y$ -  
 187 [direction due to river stage fluctuation and bank slope angle \(see the horizontal distance](#)  
 188 [between the vertical red and green solid line in Figure S2c\)](#). In contrast to [the vertical](#)  
 189 [river-bank models of](#) Gomez-Velez et al. (2017),  ~~$M(t)$  the displacement of the SWI~~  
 190 ~~caused by the deformation of the model domain ( $M(t) = [h(t) - h(0)]/\tan(\delta)$ , where  $h(t)$~~   
 191  ~~$[L]$  is transient hydraulic head)~~ is added in Eq. (1) [to simulate the models in sloping](#)  
 192 [riverbank conditions, which represents the displacement of the river boundary in  \$y\$ -](#)  
 193 [direction due to river stage fluctuation and bank slope angle \(see the horizontal distance](#)  
 194 [between the vertical red and green solid line in Figure S2c\)](#).

195 To simulate the model domain deformation and mesh displacement, we use the  
 196 DGM interface in COMSOL [Multiphysics \(COMSOL\) \(COMSOL Multiphysics, 2019\)](#).  
 197 In this interface, the deforming feature of a specified domain can be defined as a  
 198 boundary condition with a given moving velocity or displacement. DGM is based on  
 199 the arbitrary Lagrangian–Eulerian (ALE) method, which is a hybrid method that allows  
 200 both the model domain and mesh to move or deform simultaneously in a predefined  
 201 manner. More details on ALE can be found in Donea et al. (2014). While it has  
 202 previously been used for simulating general free-surface problems (e.g., Duarte et al.,  
 203 2004; Maury, 1996; Pohjoranta and Tenno, 2011), to our knowledge, DGM has not yet  
 204 been implemented to solve moving boundary problems in hyporheic exchange studies.  
 205 Here we used Eq. (1) as an input to the DGM interface to simulate the displacement of  
 206 the SWI (water flow) during a dynamic flood event. Infiltration and seepage face before  
 207 and after the peak time of the flood event, respectively, were neglected (Boano et al.,  
 208 2006; Cardenas. 2009a, b; Kruegler et al., 2020). Fig. 1 illustrates the river stage  
 209 hydrograph of this study (Fig. 1a, calculated by Eq. (S2), [where  \$t^\* = t/t\_d\$ ,  \$t\_d\$  is the](#)  
 210 [duration of flood event](#)) and the diagram of the displacement of the SWI (Fig. 1b)  
 211 during the flood event after coupling DGM into the model. The colored river boundaries  
 212 in Fig. 1b are corresponding to the times of colored dots in Fig. 1a. Additionally, solute  
 213 transport and [mean](#) RTD were simulated based on the extent of the flow field according

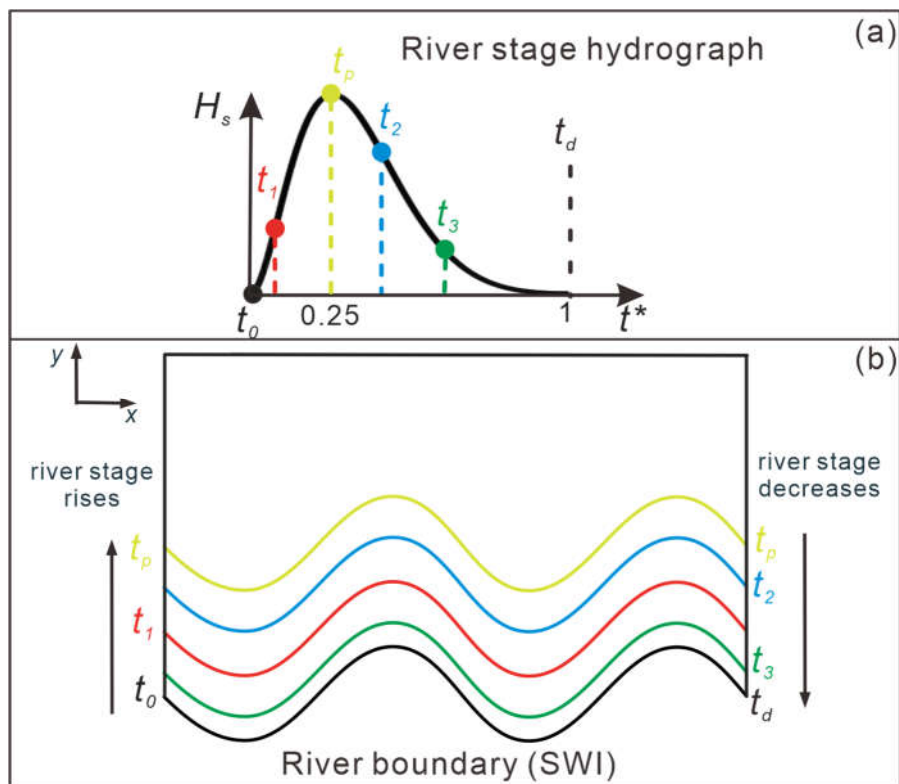
214 to Gomez-Velez et al. (2017), as shown in the SI (S2 and S3, respectively).

215

216



217



218

219 **Figure 1.** (a) River stage hydrograph during the flood event; (b) diagram showing  
 220 displacement of SWI during the flood event. The colored SWIs in (b) correspond to the  
 221 times of colored dots in (a). When the river stage increases, the river boundary migrates  
 222 into the aquifer and recovers to its initial location as river stage decreases as also  
 223 indicated by the arrows. ~~The upward and downward arrow in Fig. 1b indicates the~~  
 224 ~~raising and decreasing of river stage, respectively.~~

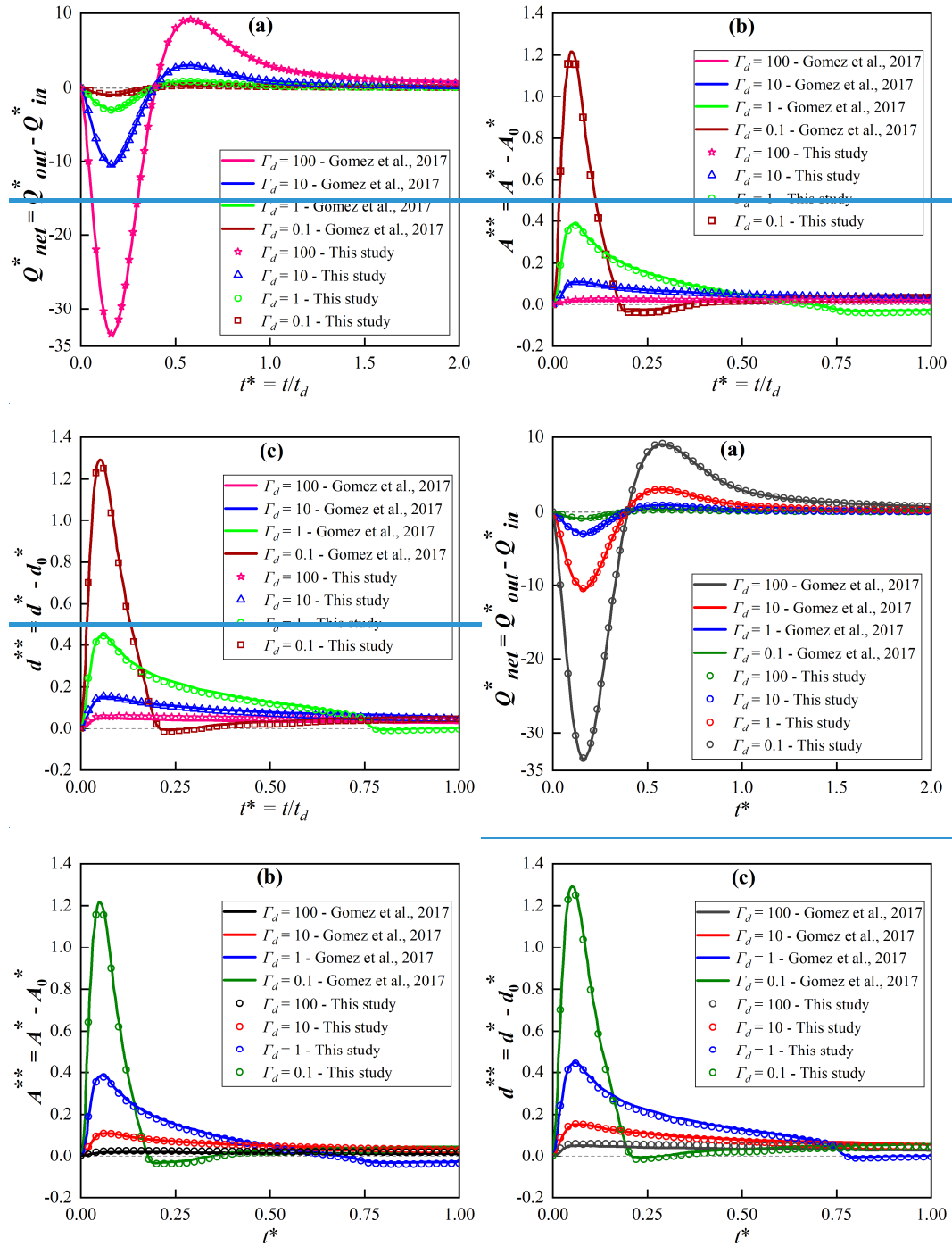
225

## 226 2.2 Model parameterization, testing and scenarios

227 Hydraulic conditions used in our numerical modeling study are based on values  
 228 from Gomez-Velez et al. (2017), who conducted a Monte Carlo analysis. They found  
 229 that the dynamic variations of HEF and mean RTD are mainly determined by ambient  
 230 groundwater flow and the ratio of aquifer hydraulic conductivity to the duration of the  
 231 flood event, — (referred to as dimensionless constant  $\Gamma_d = \frac{S_y \lambda^2}{0.5K(1+n_0)H_0 t_d}$ , (see Table 1 and  
 232 Fig. S2), where  $S_y$  is specific yield [-];  $\lambda$  is wave length of sinuous river;  $K$  is hydraulic  
 233 conductivity [ $\text{LT}^{-1}$ ];  $n_0$  is intensity of the flood event [-]  $H_0$  is base river stage [L];  $t_d$  is  
 234 duration of the flood event [T]).

235 After setting up the baseline model case with a vertical riverbank ( $\delta = 90^\circ$ ), we  
 236 compared our model results for that case with those obtained by Gomez-Velez et al.  
 237 (2017) for (a) net HEF represented by  $Q_{net, HZ}^*(t)$ ; (b) area of HZ,  $A^{**}(t)$ ; (c) penetration  
 238 of the HZ,  $d^*(t)$  for  $\Gamma_d = 0.1, 1, 10$  and  $100$ , and found that our model simulated those  
 239 cases with high accuracy (Fig. 2). Parameters  $A^{**}(t)$  and  $d^*(t)$  are based on modeling the  
 240 transport of a conservative solute while  $Q_{net, HZ}^*(t)$  is based on modeling water flow.  
 241 Slight differences between our model and that of Gomez-Velez et al. (2017) might be  
 242 due to the use of a much more refined mesh in this study as well as different length  
 243 scales.

244



245

246

247

248 **Figure 2.** Comparison of results obtained in this study with those of Gomez et al. (2017)  
 249 for the baseline case with a vertical river bank and variable  $\Gamma_d$ : (a) net hyporheic  
 250 exchange flux represented by  $Q_{net}^*(t)$ ; (b) extent of the hyporheic zone  $A^*(t)$  and (c)  
 251 penetration distance  $d^*(t)$  of the hyporheic zone into the alluvial valley. A more refined  
 252 mesh and different length scales used in this study can explain slight variations between  
 253 our model and that of Gomez et al. (2017). Information regarding model fits can be



254 found in the SI.

255

256 To test, whether our assumption of considering a vertical SWI and using the DGM  
 257 to characterize the migration of the SWI was appropriate, we compared the vertical 2-  
 258 D model with a 1-D model coupled with the DGM. Detailed information on this  
 259 comparison as well as validation results are [listed-provided](#) in the SI in section S4. The  
 260 results show that our approach is reasonable when simulating HEF in a sloping  
 261 riverbank aquifer.

262 We then considered a series of riverbank scenarios where the bank slope angle  
 263 [was varied](#), ranging from  $\delta = 90^\circ$  (vertical riverbank) to  $10^\circ$  (nearly horizontal case)  
 264 and  $\Gamma_d$  values ranged from 0.1 to 100, corresponding to aquifer hydraulic conductivity  
 265 ranging from 480 to 0.048 m/d, indicating high to low transmissivity. Table 1 presents  
 266 the parameters used in our numerical modeling study. The finite-element models  
 267 proposed in this study were set up using the COMSOL Multiphysics (COMSOL)  
 268 software. Eq. (S1), Eq. (S3) and Eq. (S6) were implemented by using [a customized](#)-  
 269 Partial Differential Equation (PDE) interface to include the Boussinesq equation,  
 270 vertical integrated solute transport equation and equation for calculating residence  
 271 (travel) time distributions (RTD), respectively. The model domain was discretized into  
 272 about 0.5 million variably-sized triangular elements, with refinement imposed near the  
 273 river boundary. Mesh-independent numerical solutions are achieved by limiting grid  
 274 size ( $\Delta L$ ) to less than 0.2 m. Thus, the transverse and longitudinal Peclet numbers  
 275 (calculated by  $Pe = \Delta L / \alpha_L$  and  $Pe = \Delta L / \alpha_T$ , respectively) in both advection and diffusion  
 276 dominated zones are less than 1, which is smaller than the upper limit of  $Pe = 4$  to  
 277 effectively avoid numerical oscillations and instabilities.

278

279 **Table 1.** Parameters and values used in our numerical model simulations.

Parameters	Value	Description
Constant model parameters		

$S_y$	0.3	Specific yield [-]
$\lambda$	40	River boundary wave length [L]
$\alpha$	5	River boundary amplitude [L]
$\theta$	0.3	Efficient porosity [-]
$J_x$	0.0025	Base groundwater gradient [-]
$\sigma$	1.14	River boundary sinuosity [-]
$t_d$	10	Duration of flood event [T]
$n_d$	0.25	Skewness of flood event [-]
$t_p$	$n_d t_d$	Time to peak river stage [T]
$H_0$	1	Base river stage [L]
$n_0$	1	Intensity of flood event [-]
$\alpha_L$	2	Longitudinal dispersivity [L]
$\alpha_T$	$0.1 \alpha_L$	Transverse dispersivity [L]
Variable model parameters		
$\Gamma_d$	0.1 1 10 100	Dimensionless aquifer transmissivity [-]
$\delta$	90 70 50 20 10	Bank slope angle [°]

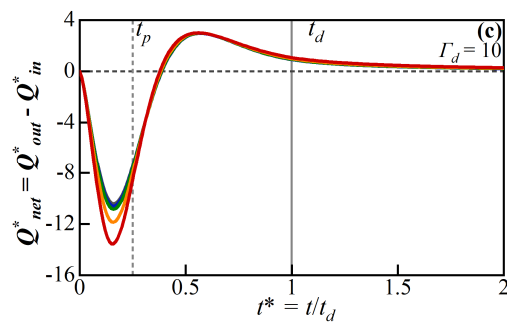
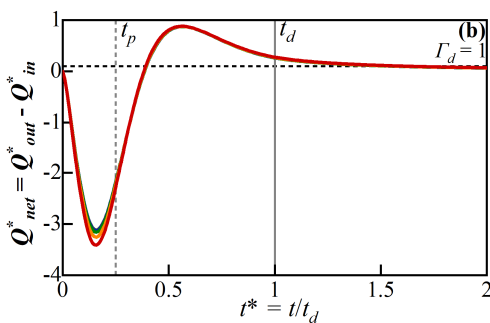
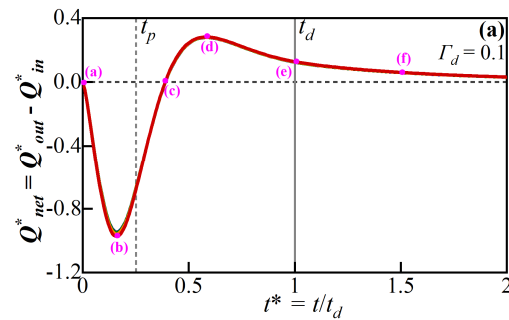
280

281 —Similar to Gomez-Velez et al. (2017), we evaluated the impact of bank slope  
 282 by comparing the net hyporheic exchange flux ( $Q_{net, HZ}^*(t)$ ), area of HZ ( $A^{**}(t)$ ),  
 283 penetration distance of the HZ ( $d^{**}(t)$ ) and mean RTD ( $\mu_r^*(\mathbf{x}, t)$ ) between vertical and  
 284 sloping river bank models. A detailed definition of these variables is provided in the SI  
 285 (section S5).

286

287 **3. Results**288 **3.1 Effect of bank slope on hyporheic exchange flow and HZ extent**289 **3.1.1 Hyporheic exchange flow**

290 The flow field (velocity magnitude and direction) and net HEF ( $Q_{net, HZ}^*(t)$ )  
 291 changed dynamically during and after the simulated flood event. Fig. 3a – 3d show the  
 292 progression evolution of net HEF for different aquifer transmissivity ( $\Gamma_d$ ) and bank  
 293 slope angle ( $\delta$ ) conditions. Snapshots of the flow field and the boundary of the HZ area  
 294 (isolines of  $C(\mathbf{x}, t) = 0.5$  as concentration of a conservative solute) for different  $\delta$   
 295 conditions at different times (pink dots in Fig. 3a) for  $\Gamma_d = 1$  are shown in Fig. 4a - 4f.  
 296



299

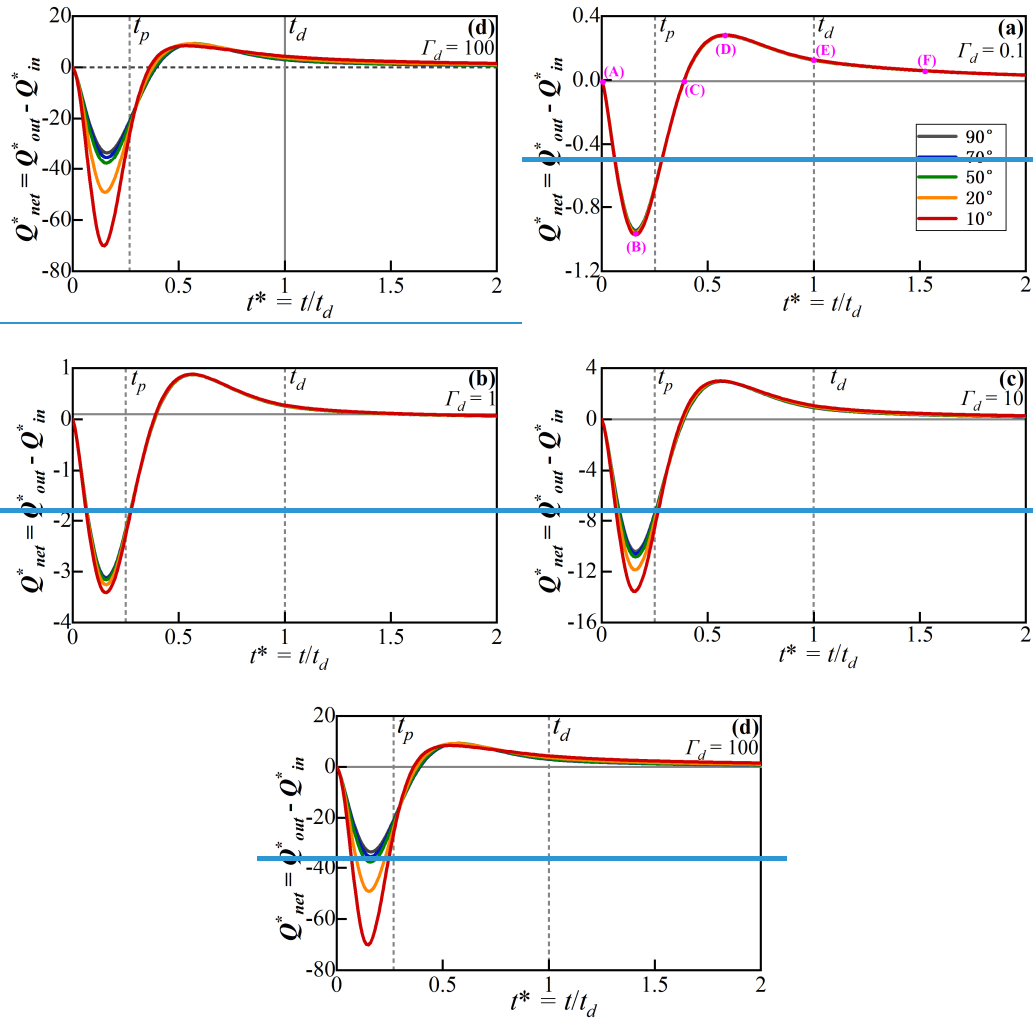
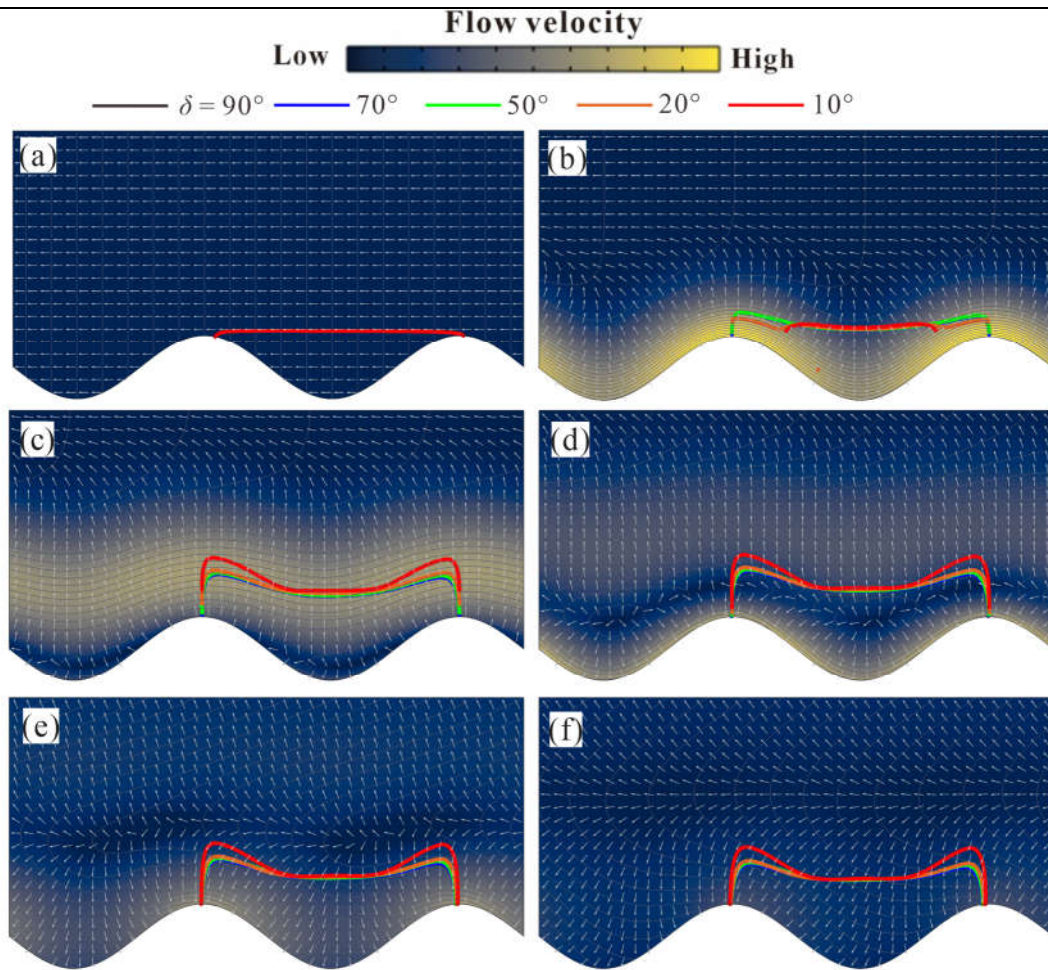


**Figure 3.** Temporal progression evolution of dimensionless net HEF ( $Q_{net, HZ}^*(t)$ ) for four different aquifer transmissivity values (represented by  $\Gamma_d$ ) and bank slopes angles ( $\delta$ , from 10-90 degrees). Time-to-peak flood ( $t_p$ ) and flood duration ( $t_d$ ) are marked by vertical dashed lines. Pink dots in (a) marked by (aA) - (fF) correspond to the snapshots of the flow field shown in Fig. 4. A negative flux value here represents water flow from the river to the aquifer. Note that  $\Gamma_d$  negatively correlates with the transmissivity of the aquifer.



311  
 312 **Figure 4.** Plan view of the river channel and aquifer showing the temporal progression  
 313 evolution of the alluvial flow field and spatial extent of the HZ. (a)-(e) are snapshots of  
 314 the flow field at different time steps ( $t^* = 0, 0.16, 0.39, 0.57, 1, 1.5$ ) during the simulated  
 315 event (pink dots in Fig. 3a). Colored surfaces represent the magnitude of the Darcy flux  
 316 vector (blue is low and yellow is high) and white isolines the dimensionless hydraulic  
 317 head. Bold colored lines correspond to the HZ extent for different bank slope  
 318 conditions.

319

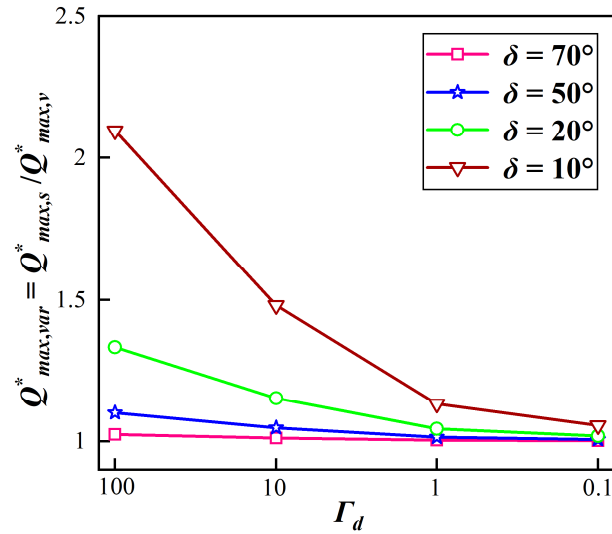
320

321 Before the flood event ( $t = 0$ ), steady-state base flow conditions are assumed, as  
 322 shown in Fig. 4a. The inflow and outflow (along the upstream and downstream meander  
 323 bend, respectively) are in balance. The bank slope has no effect on the HZ boundaries  
 324 before the flood event.

325 Before peak river stage of the flood event is reached ( $0 < t < 0.25t_d$ ), the onset of  
 326 the flood event is indicated by the rising river stage and forces the river to infiltrate into  
 327 the aquifer along the SWI (negative values of  $Q_{net, HZ}^*(t)$  in Fig. 3), resulting in the  
 328 expansion of the HZ as shown in Fig. 4b. The influx of river water into the HZ ( $-Q_{net, HZ}^*(t)$ )  
 329 reaches its maximum before the time-to-peak river stage ( $t = 0.25t_d$ ) because the  
 330 pressure wave propagates into the aquifer and decreases the head gradient between the  
 331 river and the connected aquifer. For higher transmissivity aquifers (Lower  $\Gamma_d$  values in  
 332 Fig. 3), bank slope has a reduced impact on net outflux as the fast propagation of the  
 333 pressure wave results in the hydraulic head near the SWI to be very similar. Among  
 334 different aquifer transmissivity conditions. As aquifer transmissivity decreases, the  
 335 ability of the aquifer to transmit the pressure wave becomes limited, and the interaction  
 336 flux is dominated by the location (displacement) of the SWI and the river stage. On the  
 337 other hand, a smaller slope angle induces a longer displacement of the SWI ( $M(t)$ ) away  
 338 from the river, where the groundwater head adjacent to the SWI is always relatively  
 339 high (i.e., the head in base flow condition). This, consequently, leads to a larger head  
 340 gradient near the SWI as well as larger dimensionless net fluxes under increasing  $\Gamma_d$   
 341 conditions as shown in Fig. 3.

342 The maximum dimensionless flux ratios  $Q_{max, var}^* = Q_{max, s}^* / Q_{max, v}^*$  of sloping ( $\delta$   
 343  $< 90^\circ$ ,  $Q_{max, s}^*$ ) vs vertical ( $\delta = 90^\circ$ ,  $Q_{max, v}^*$ ) riverbank cases are shown in Fig. 5, which  
 344 indicates the deviation in predicting peak net flux when neglecting the slope of the  
 345 riverbank. The bank slope is found to increase infiltration by up to 120% ( $Q_{max, var}^* \approx$   
 346 2.2) for  $\Gamma_d = 100$  with  $\delta = 10^\circ$  while for larger slope angles or higher hydraulic  
 347 transmissivities the dimensionless infiltration gradually decreases.

348



349

350 **Figure 5.** Ratio of maximum net flux for slope to no-slope (vertical river bank)351 conditions  $Q_{max,var}^* = Q_{max,s}^* / Q_{max,v}^*$  for four aquifer transmissivities and slope angles.352 Note that  $\Gamma_d$  negatively correlates with aquifer transmissivity.

353

354

355 As the river stage decreases after  $t_p$ , the head gradient near the SWI gradually

356 reverses and the net outflux starts increasing (the river is gaining water) as shown in

357 Fig. 3. This is associated with the river stage declining below the groundwater level

358 (see Fig. 4c - 4f). For the lowest hydraulic transmissivity condition ( $\Gamma_d = 100$ ), bank

359 slope can slightly extend the time required for the system to recover to initial conditions

360 after  $t_p$  but in general, the response of the net outflux to bank slope is negligible when

361 compared to that of the influx. Eventually, the net flux converges to zero, which

362 indicates the flow field within the aquifer recovers to the initial conditions. The bank

363 slope has no impact on the HEF after the duration of [the](#) flood event.364 **3.1.2 Patterns of hyporheic area and penetration distance**365 Fig. 6 and Fig. 7 show the temporal [evolution-progression](#) of the dimensionless366 HZ area ( $A^{**}(t)$ ) and penetration distance ( $d^{**}(t)$ ) into the alluvial valley relative to the367 initial condition for varying aquifer transmissivity ( $\Gamma_d$ ) and slope angles.

368

369

370

371

372

373

374

375

376

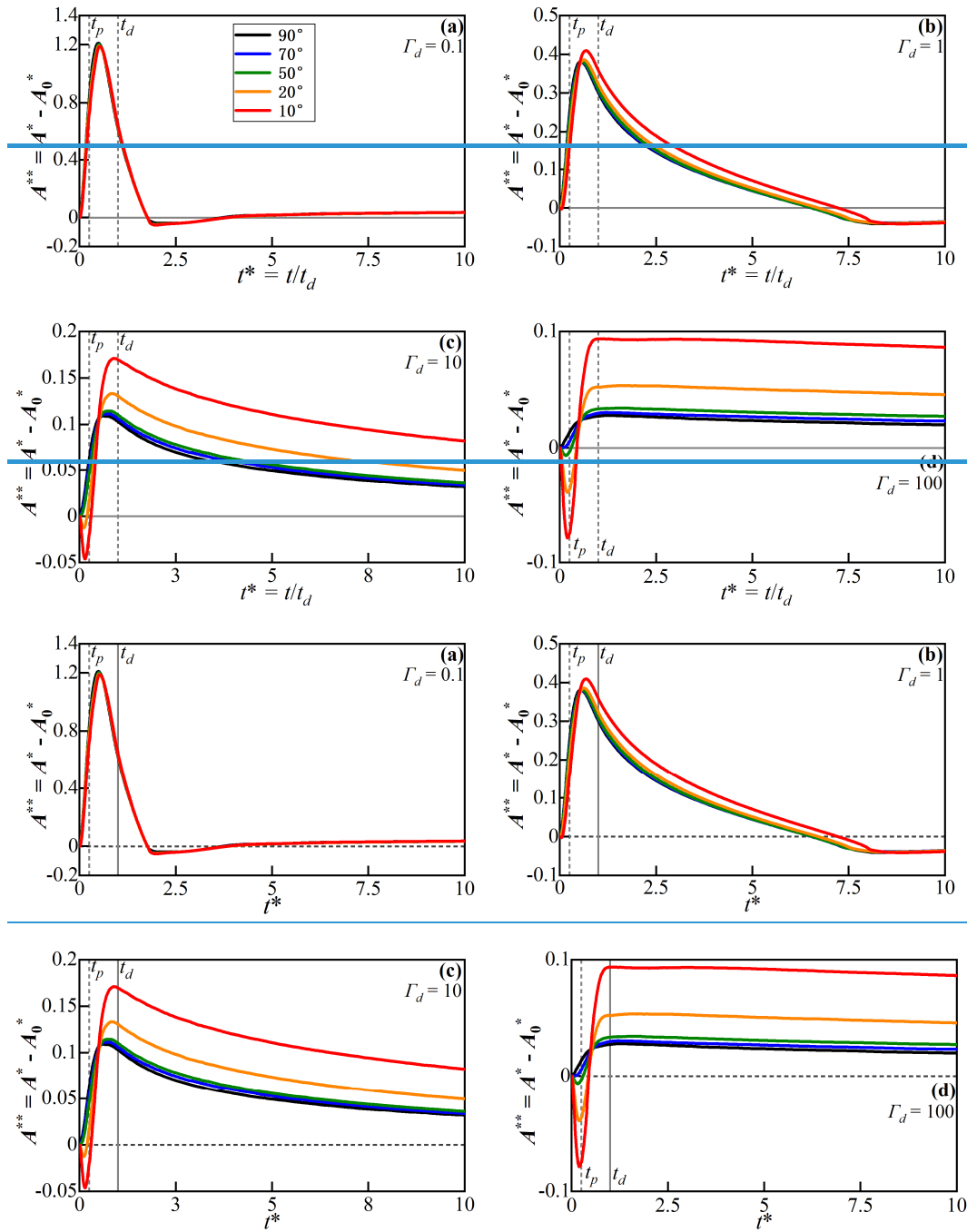


**Figure 6.** Temporal progression evolution of dimensionless HZ area for different values of  $\Gamma_d$  and  $\delta$  (colored lines). Time-to-peak ( $t_p$ ) and flood duration ( $t_d$ ) are marked by vertical dashed lines.



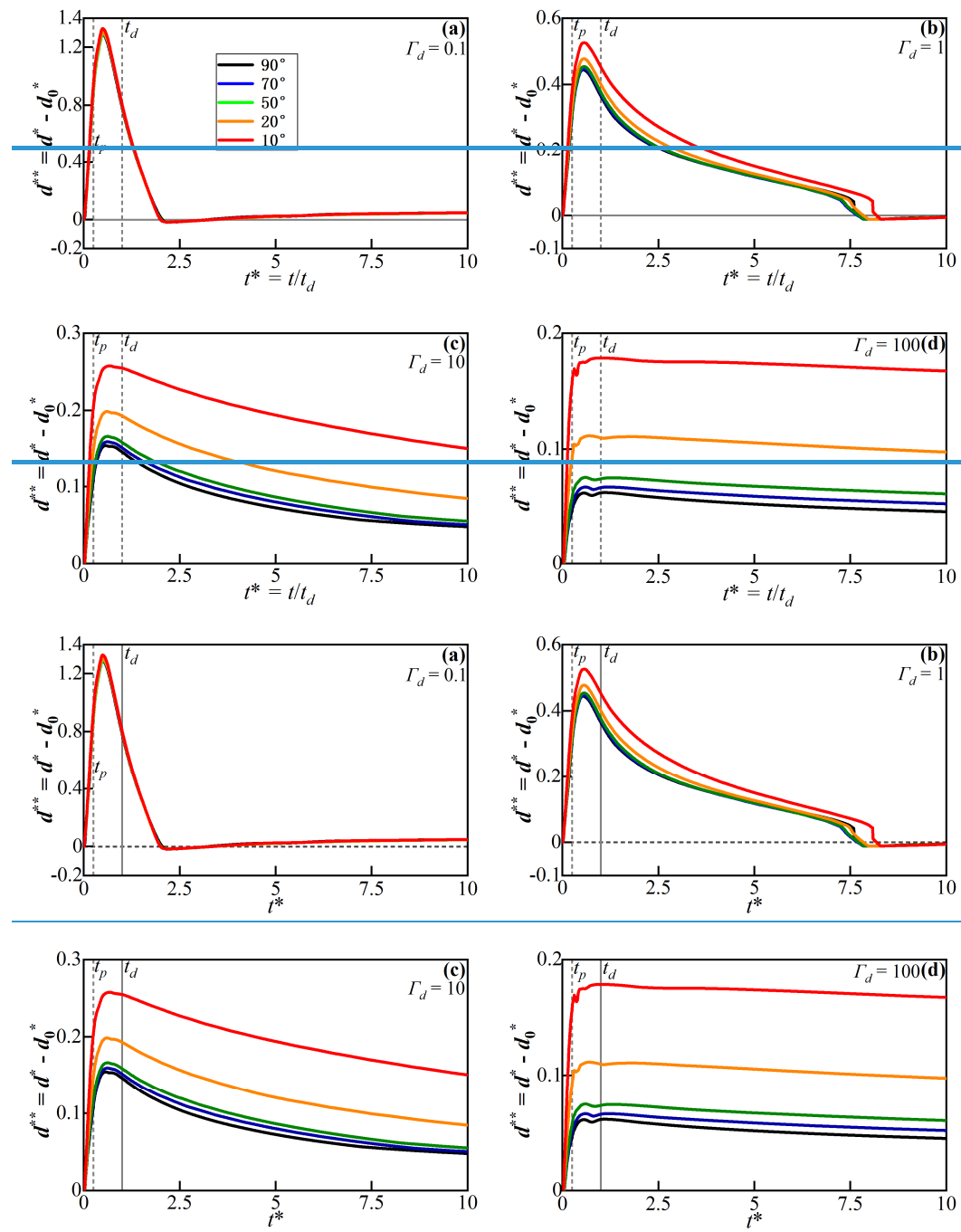


**Figure 7.** Temporal progression evolution of dimensionless HZ penetration distance into the alluvial valley ( $d^{**}$ ) for different values of  $\Gamma_d$  and  $\delta$  (color lines). Time-to-peak ( $t_p$ ) and flood duration ( $t_d$ ) are marked by vertical dashed lines.

For vertical banks ( $\delta = 90^\circ$ , black lines in Fig. 6), the HZ area increases synchronously with the river stage ( $t < t_p$ ). After the peak time of the flood event ( $t >$

388  $t_p$ ), the HZ area continues to extend as river water still recharges the aquifer. After the  
 389 flood event ( $t > t_d$ ), the river water that was stored in the aquifer ( $C(\mathbf{x}, t) > 0$ ) slowly  
 390 discharges back into the river channel. Thus, the HZ area and penetration distance  
 391 gradually rebound to initial conditions.

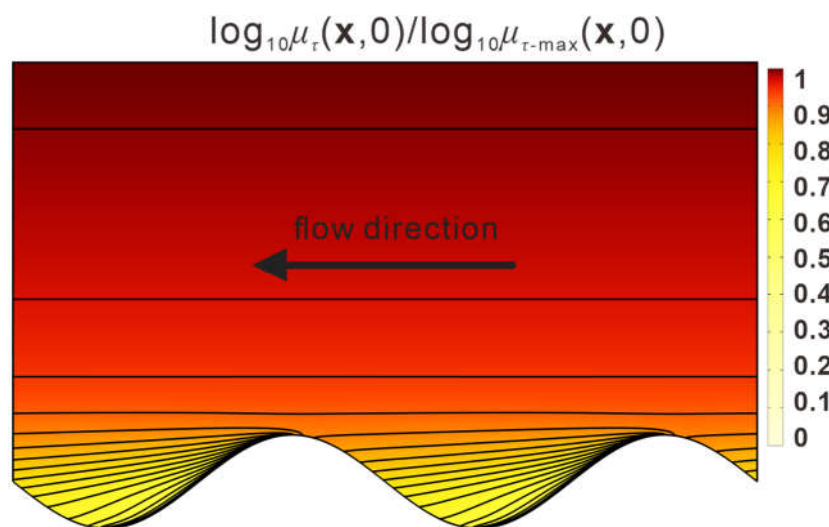
392 Under sloping riverbank conditions, the riverbank will at times be submerged by  
 393 the rising river stage. Fig. 6a and 7a show that the effects of bank slope on HZ area  
 394 ( $A^{**}(t)$  in Fig. 6) and penetration distance ( $d^{**}(t)$  in Fig. 7) are almost counteracted by  
 395 the high transmissivity of the aquifer while ~~and~~ the influence of bank slope was  
 396 negligible. At the beginning of the flood event, Fig. 6b – 6d show that for conditions  
 397 with smaller sloping angle, HZ area can be less than zero (HZ at these times are smaller  
 398 than the initial condition). This is due to the fact that the movement of the SWI during  
 399 a rising river stage towards the alluvial valley will submerge parts that were previously  
 400 unsaturated as the aquifer with low transmissivity will propagate water more slowly.  
 401 As aquifer transmissivity decreases from Fig. 6b – 6d, the relative HZ area remains  
 402 negative for a longer time for smaller bank slopes. This indicates that bank slope has a  
 403 more pronounced effect on HZ extent in cases where aquifer transmissivity is large as  
 404 a low-transmissivity aquifer takes more time to propagate infiltrating river water.

405 After about half the flood duration ( $t > 0.5t_d$ ), the HZ area ( $A^{**}$ ) becomes positive  
 406 in all scenarios as the model domain previously submerged during the flood event re-  
 407 emerges. As aquifer transmissivity decreases (Fig. 6a – 6d and Fig. 7a – 7d), the impact  
 408 of bank slope gradually increases especially in low aquifer transmissivity conditions,  
 409 where smaller bank slope can increase the peak values of area and penetration distance,  
 410 and delay the arrival time-to-peak value of the relative HZ area. After the flood event  
 411 ( $t > t_d$ ), the effect of bank slope is counteracted by the higher aquifer transmissivity and  
 412 only lower transmissivities have a significant impact on the HZ resulting in larger  $A^{**}(t)$   
 413 and  $d^{**}(t)$  as shown in Fig. 6b – 6d and Fig. 7b – 7d. For low transmissivity scenarios,  
 414 the bank slope can increase the peak area and penetration of the HZ by almost 200%.

### 415 3.2 Spatiotemporal progression evolution of mean residence time distribution

416 The progression evolution of spatiotemporal patterns of mean RTD (i.e., travel  
 417 time of river water in aquifer) is a useful evaluation method for identifying the dynamic  
 418 variation of aging and rejuvenation of hyporheic water. Here we use the mean RT ratio  
 419 between a sloping model and a vertical model  $\mu_r^*(\mathbf{x}, t) = \log_{10}(\mu_{\tau-S}(\mathbf{x}, t)/\mu_{\tau-V}(\mathbf{x}, 0))$  to  
 420 evaluate the influence of bank slope on the prediction of mean RTD for a given location  
 421 and time. Fig. 8 presents mean RTDs for the initial condition, where  $\mu_{\tau 0-\max}$  is the  
 422 maximum RT in the domain. It can be seen that the isolines representing the RT are  
 423 almost horizontal in the area extending from the river but RT near the upstream river  
 424 bend is smaller than downstream because the initial flow direction is towards the  
 425 negative direction of the  $x$  axis. Notably,  $\mu(\mathbf{x}, 0)$  grows almost exponentially as  $y$   
 426 increases, and a positive correlation to  $\Gamma_d$  at a given location is observed.

427



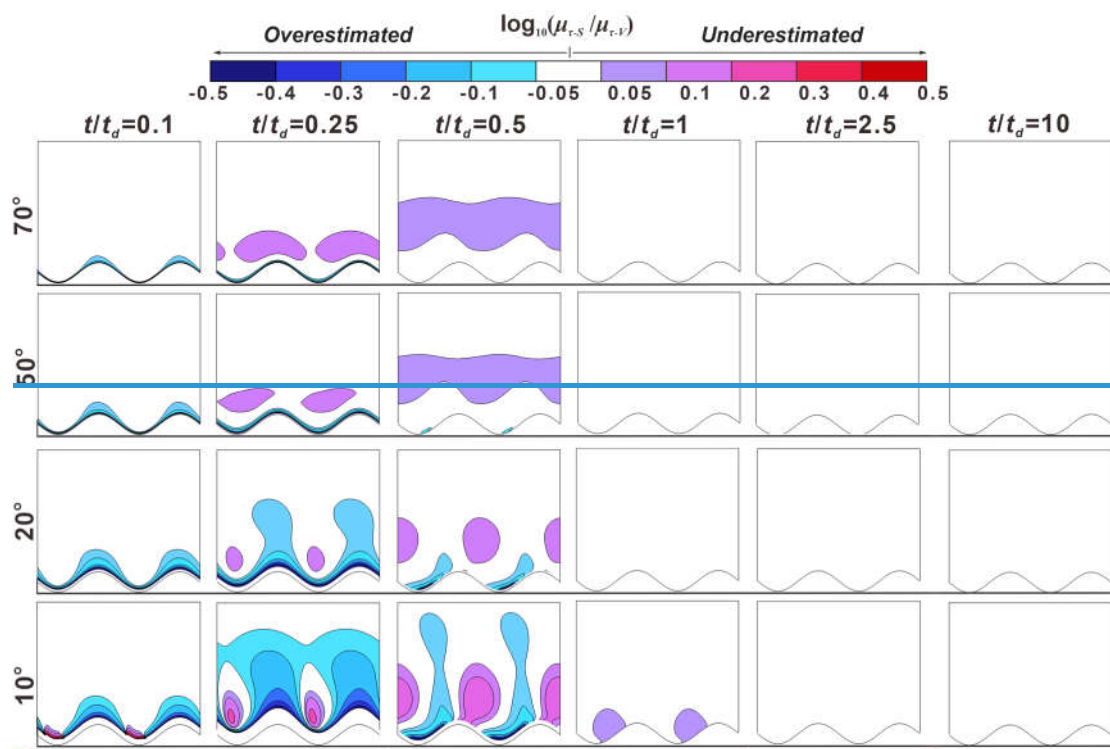
428

429 **Figure 8.** Plain view of rRelative mean residence time distributions [-] for baseline flow  
 430 conditions (no bank slope), which are represented by  $\log_{10}\mu_{\tau}(\mathbf{x}, 0)/\log_{10}\mu_{\tau-\max}(\mathbf{x}, 0)$  to  
 431 show the distribution pattern. The value of the contour lines grows exponentially with  
 432 the distance from the river meander.

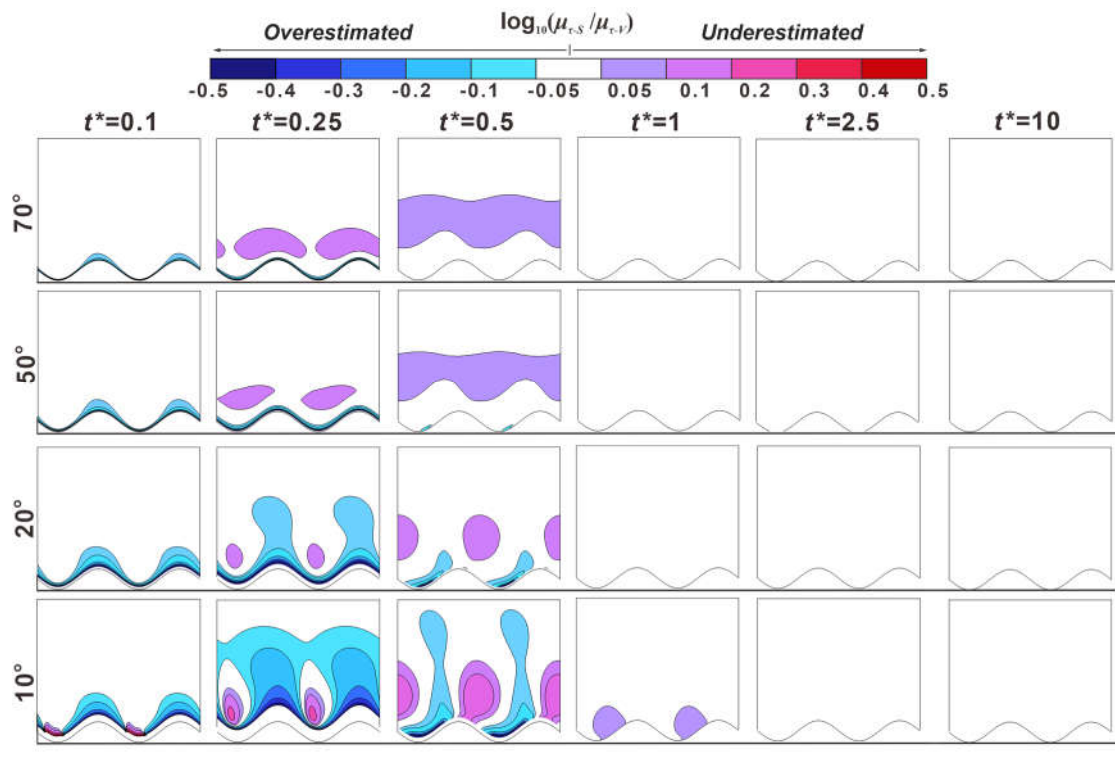
433

434 Fig. 9 - 12 present five snapshots of  $\mu_r^*$  for different bank slope angles and different

435 aquifer transmissivity [aquifers values](#) ( $T_d = 0.1, 1, 10$  and  $100$ , respectively). The five  
 436 snapshots represent the rising limb of the flood event ( $t^*/t_d = 0.1$ ), the peak of the flood  
 437 event ( $t^*/t_d = 0.25$ ), the falling limb of the flood event ( $t^*/t_d = 0.5$ ) and a time after the  
 438 flood event ( $t^*/t_d = 1, 2.5$  and  $10$ ). The [RT-differences in residence time](#) between  
 439 sloping and vertical riverbank models are within 12.2% in the white-colored areas ( $-$   
 440  $0.05 < \mu_r^* < 0.05$ ) of Fig. 9 - 12, which indicates a minor effect of bank slope on [mean](#)  
 441 RTD. The colored areas in Fig. 9 - 12 indicate model results where neglecting bank  
 442 slope will lead to [an overestimation](#) ( $\mu_r^* < -0.05$ ) or [underestimation](#) ( $\mu_r^* > 0.05$ ) of  
 443 residence (travel) times.



444



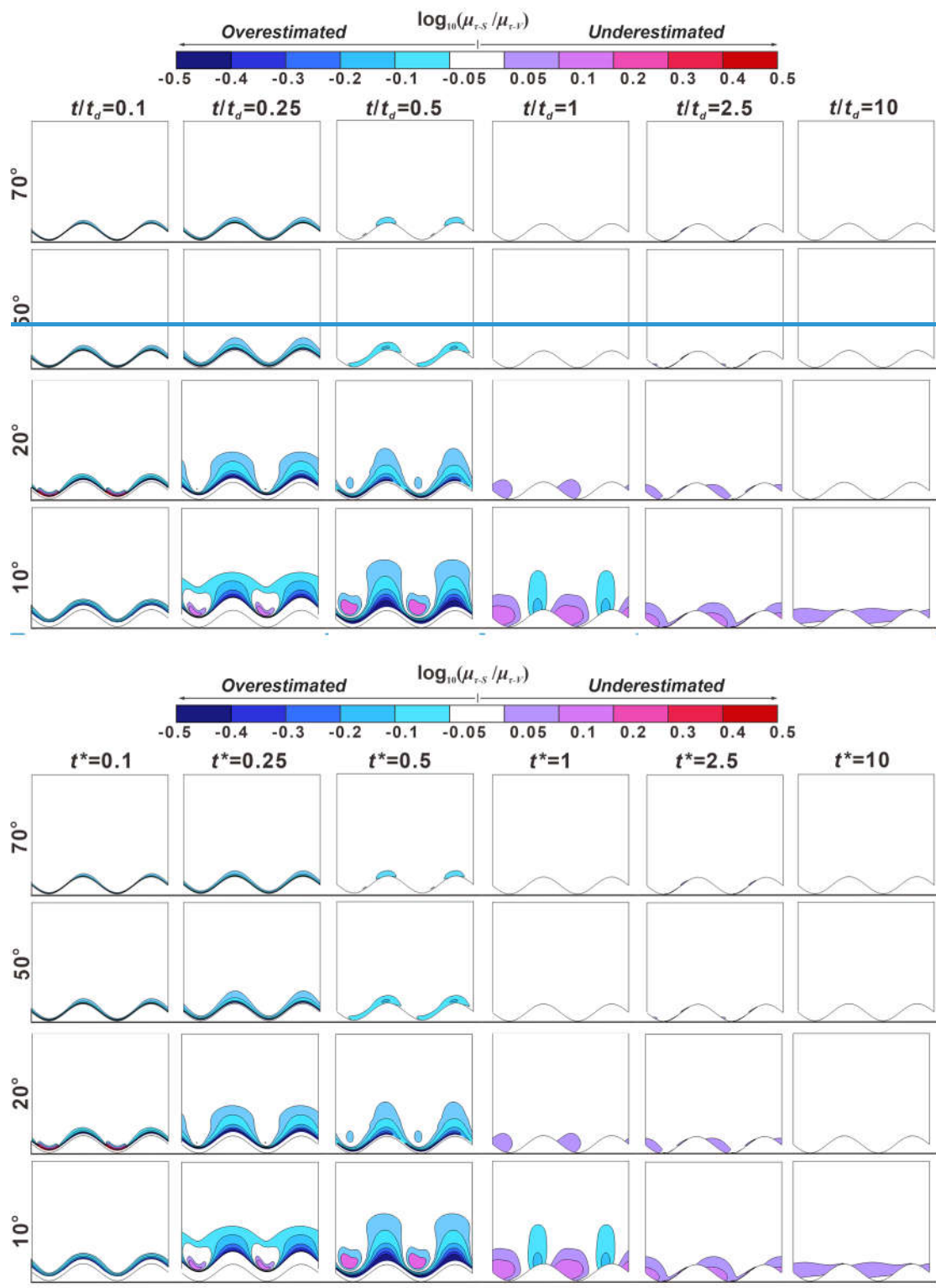
445

446 **Figure 9.** Five snapshots for the mean RTD ratio ( $\mu_r^*(\mathbf{x}, t) = \mu_{r-S}^*(\mathbf{x}, t) / \mu_{r-V}^*(\mathbf{x}, t)$ )  
 447 between sloping ( $\mu_{r-S}^*(\mathbf{x}, t)$ ) and vertical riverbank conditions ( $\mu_{r-V}^*(\mathbf{x}, t)$ ) at different  
 448 times  $t^*/t_d$  as a function of  $\delta$  for  $\Gamma_d = 0.1$ . The horizontal lines beneath each figure are  
 449 the reference lines to show the initial location of the peak point of the point bar. The  
 450 lower sinuous lines at the reference lines are the initial SWIs. The colored areas indicate  
 451 where the bank slopes have significant impact on RT (difference in RT between sloping  
 452 and vertical model larger than 12.2%) and residence (travel) times of river water in the  
 453 aquifer would be overestimated

454 (cold color area) or underestimated (warm color area) if the effect of the bank slope was  
 455 ignored.

456 or underestimated.

457

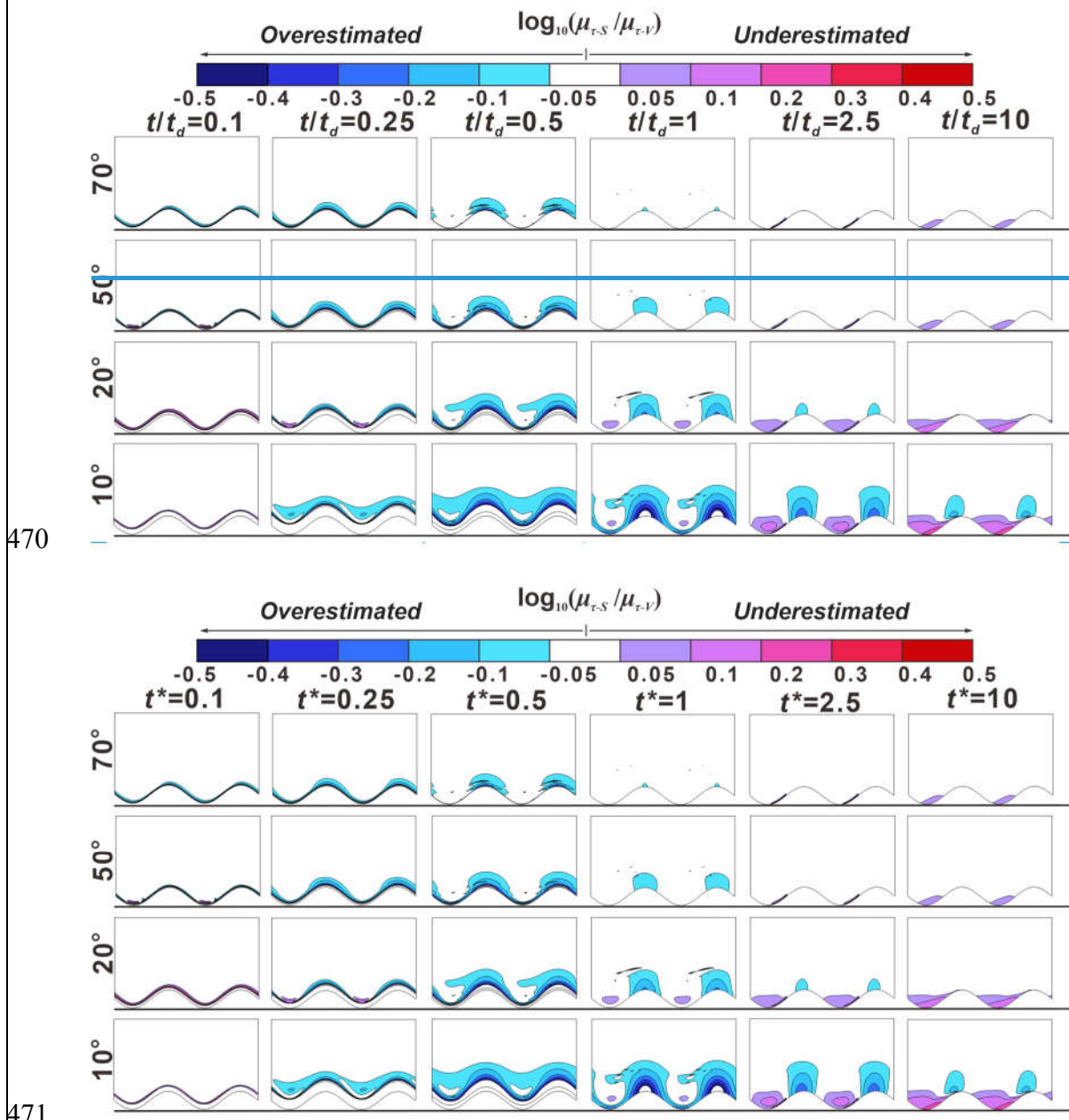


458

459

460 **Figure 10.** Five snapshots for the mean RTD ratio ( $\mu_r^*(\mathbf{x}, t) = \mu_{r-S}^*(\mathbf{x}, t) / \mu_{r-V}^*(\mathbf{x}, t)$ )  
 461 between sloping ( $\mu_{r-S}^*(\mathbf{x}, t)$ ) and vertical riverbank conditions ( $\mu_{r-V}^*(\mathbf{x}, t)$ ) at different  
 462 times  $t^*/t_d$  as a function of  $\delta$  for  $\Gamma_d = 1$ . The horizontal lines beneath each figure are the  
 463 reference lines to show the initial location of the peak point of the point bar. The lower

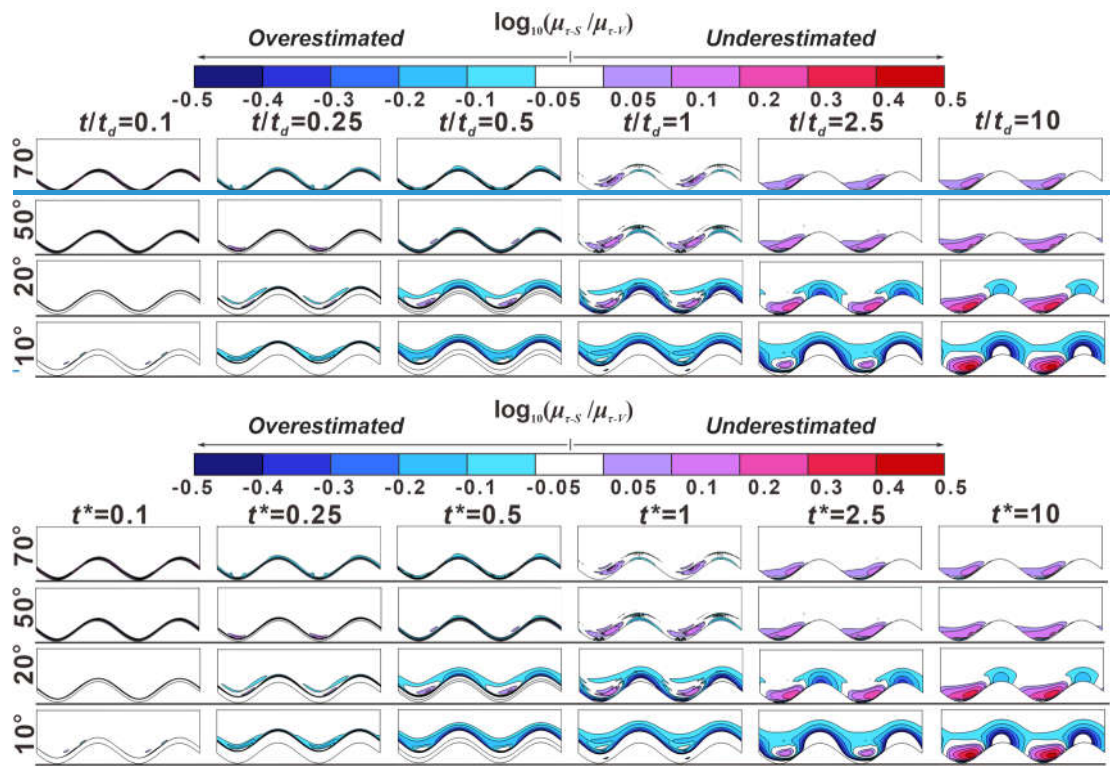
464 sinuous lines at the reference lines are the initial SWIs. The colored areas indicate where  
 465 the bank slopes have significant impact on RT (difference in RT between sloping and  
 466 vertical model larger than 12.2%) and residence (travel) times of river water in the  
 467 aquifer would be overestimated (cold color area) or underestimated (warm color area)  
 468 [if the effect of the bank slope was ignored, or underestimated](#)  
 469



471  
 472 **Figure 11.** Five snapshots for the [mean](#) RTD ratio ( $\mu_r^*(\mathbf{x}, t) = \mu_{r-S}^*(\mathbf{x}, t) / \mu_{r-V}^*(\mathbf{x}, t)$ )  
 473 between sloping ( $\mu_{r-S}^*(\mathbf{x}, t)$ ) and vertical riverbank conditions ( $\mu_{r-V}^*(\mathbf{x}, t)$ ) at different

474 times  $t^*/t_d$  as a function of  $\delta$  for  $\Gamma_d = 10$ . The horizontal lines beneath each figure are  
 475 the reference lines to show the initial location of the peak point of the point bar. The  
 476 lower sinuous lines at the reference lines are the initial SWIs. The colored areas indicate  
 477 where the bank slopes have significant impact on RT (difference in RT between sloping  
 478 and vertical model larger than 12.2%) and residence (travel) times of river water in the  
 479 aquifer would be overestimated (cold color area) or underestimated (warm color area)  
 480 [if the effect of the bank slope was ignored or underestimated](#)

481



482

483

484 **Figure 12.** Five snapshots for the [mean](#) RTD ratio ( $\mu_r^*(\mathbf{x}, t) = \mu_{r-S}^*(\mathbf{x}, t) / \mu_{r-V}^*(\mathbf{x}, t)$ )  
 485 between sloping ( $\mu_{r-S}^*(\mathbf{x}, t)$ ) and vertical riverbank conditions ( $\mu_{r-V}^*(\mathbf{x}, t)$ ) at different  
 486 times  $t^*/t_d$  as a function of  $\delta$  for  $\Gamma_d = 100$ . The horizontal lines beneath each figure are  
 487 the reference lines to show the initial location of the peak point of the point bar. The  
 488 lower sinuous lines at the reference lines are the initial SWIs. The colored areas indicate  
 489 where the bank slopes have significant impact on RT (difference in RT between sloping  
 490 and vertical model larger than 12.2%) and residence (travel) times of river water in the  
 491 aquifer would be overestimated ([cold color area](#)) or underestimated ([warm color area](#))



492 if the effect of the bank slope was ignored or underestimated

493  
494  
495 At  $t^*/t_d = 0.1$ , a smaller bank slope can lead to a shorter travel time of river water  
496 in the aquifer (negative values of  $\mu_r^*$ ) near the SWI compared to the vertical riverbank  
497 scenario. The area of shorter travel time caused by bank slope was positively related to  
498 aquifer transmissivity. The effect of bank slope is small for  $\Gamma_d = 10$  and  $100$  because the  
499 groundwater mound (the raised groundwater stage) piles up around the river boundary,  
500 but that small area extended deeper into the alluvial valley for smaller slope angles.  
501 Due to the scattered and nested flow paths near the cut bank and point bar, respectively,  
502 the area of the negative value of  $\mu_r^*$  at the cut bank of the SWI is larger than that at the  
503 point bar. The change of flow direction near the point bar leads to a prolonged flow path  
504 for the water in the river channel as well as to forced groundwater mixing with the  
505 slightly older water (as shown in Fig.8 shows that the water was more aged potentially  
506 older in  $y$  direction compared to  $-x$  direction in the point bar). This effect was amplified  
507 with decreasing bank slope angle, but it is only statistically significant ( $\mu_r^* < -0.05$  or  
508  $\mu_r^* > 0.05$ ) when  $\delta = 10^\circ$  at  $t^*/t_d = 0.1$ .

509 At the time of peak flood ( $t^*/t_d = 0.25$ ), the river still infiltrates into the aquifer.  
510 For  $\Gamma_d = 0.1$ , results of  $\mu_r^*$  in Fig. 9 show that bank slope can lead to both overestimated  
511 and underestimated RT areas. Both magnitude of relative RT ( $\mu_r^*$ ) and associated area  
512 increase with decreasing slope due to the longer travel distance of river water into the  
513 aquifer. As the slope angle decreases, the underestimated travel time area was located  
514 closer to the peak of the cutbank. The impact of bank slope on mean RTD for  $\Gamma_d = 1$   
515 was rather similar in its pattern compared to  $\Gamma_d = 0.1$ , but the degree of that impact was  
516 reduced. For  $\Gamma_d = 10$  and  $100$ , only overestimated travel time area can be seen near the  
517 river bank with a smaller area of impact compared to smaller  $\Gamma_d$  conditions, because the  
518 groundwater has not sufficiently propagated into the aquifer due to lower transmissivity.

519 At  $t^*/t_d = 0.5$ , part of the aquifer that was submerged at  $t^*/t_d = 0.25$  reemerges

520 due to the decline in river stage. In most cases, smaller bank slopes can lead to wider  
 521 reemergence of the aquifer, which therefore results in overestimated travel time area  
 522 near the river boundary; however, this was not the case for  $\Gamma_d = 0.1$  where bank slope  
 523 can both lead to overestimated and underestimated ~~travel-time~~RT area. Furthermore,  
 524 compared to when  $t^*/t_d = 0.25$ , the impact of bank slope becomes weaker for  $\Gamma_d = 0.1$ ,  
 525 but more relevant for the larger  $\Gamma_d$  values.

526 After the flood event ( $t^*/t_d > 1$ ), the influence of bank slope on mean travel time  
 527 is nearly eliminated for  $\Gamma_d = 0.1$  and 1 due to the high aquifer transmissivity. However,  
 528 for aquifers with lower transmissivity ( $\Gamma_d = 10$  and 100), bank slope still has a  
 529 significant effect on RT at  $t^*/t_d = 10$  and leads to underestimated and overestimated RT  
 530 areas near the point bar and the cut bank, respectively.

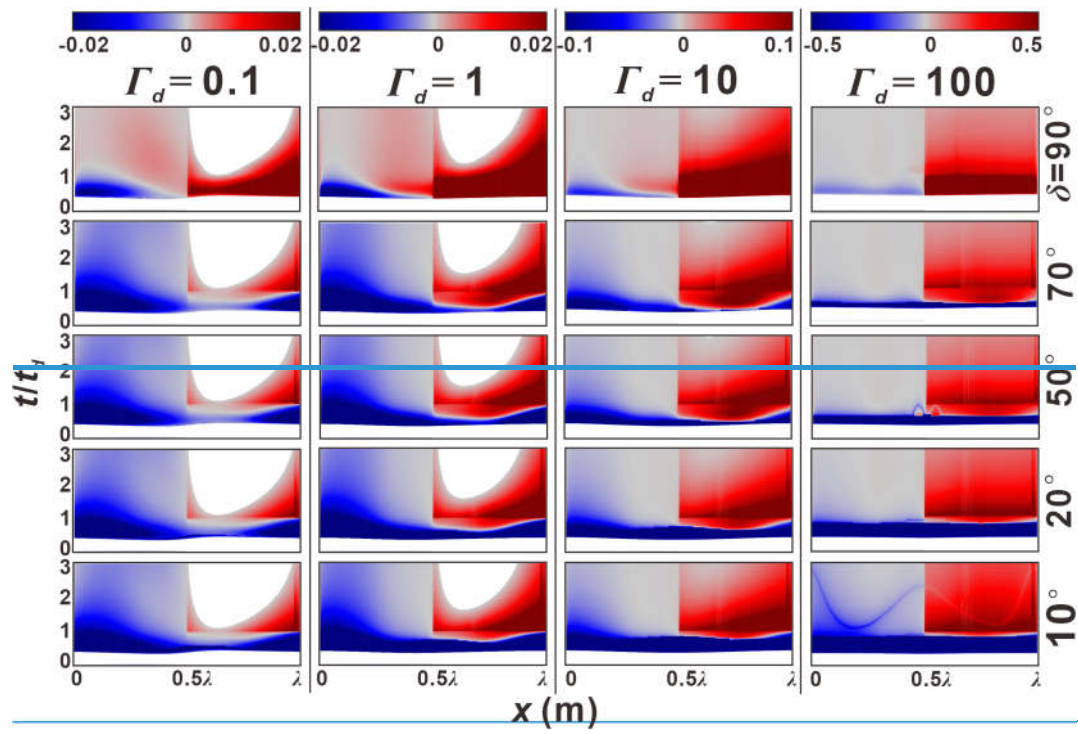
531 Overall, Fig. 9-12 indicate that the time when bank slope was relevant in predicting  
 532 RT (travel time of groundwater in aquifer) was determined by the transmissivity of the  
 533 aquifer. For ~~higher transmissivity~~more transmissive aquifers, the impact of bank slope  
 534 on the prediction of groundwater travel time cannot be neglected during the flood event  
 535 ( $0 < t < t_d$ ), but that impact will be eliminated after the flood event due to the quickly  
 536 recovery of the aquifer to the basebaseline conditions. For lower transmissivity aquifers,  
 537 bank slope plays an important role on groundwater travel time after ~~the half-time-of~~  
 538 ~~flood event~~ ( $t > 0.5 * t_d$ ) and has a more lasting influence on aquifer RT, as more time is  
 539 required to recover to initial conditions for lower transmissivity aquifer.

### 540 3.3 Relative flux-weighted residence time

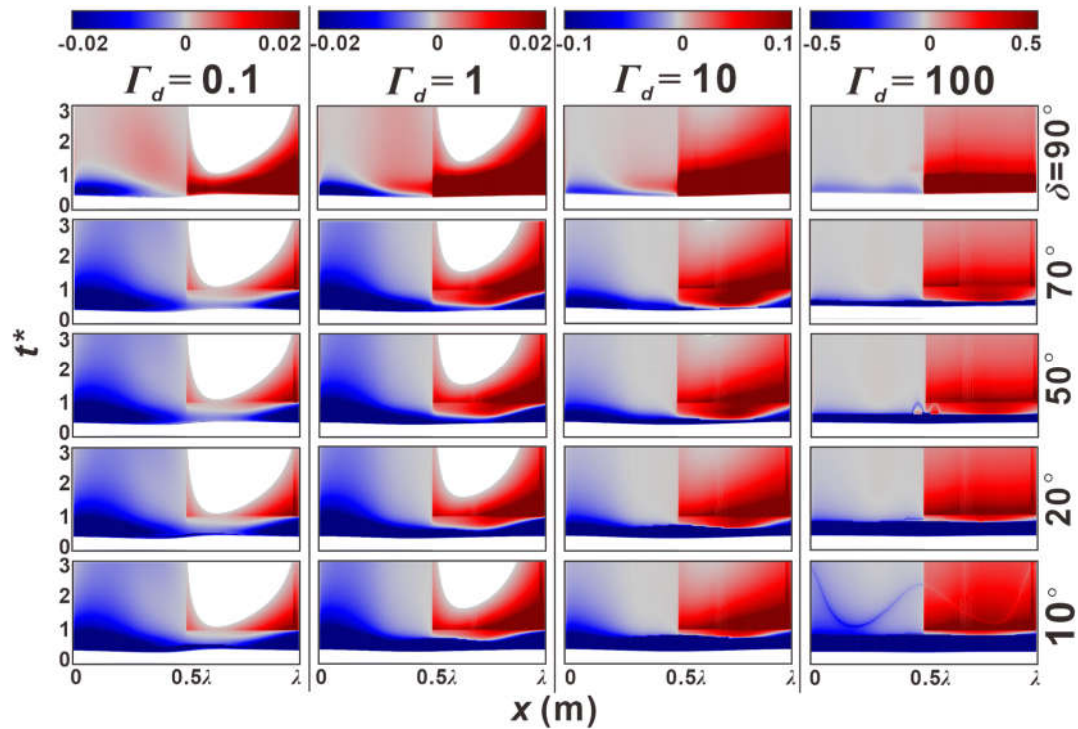
541 Fig. 13 shows the ~~progression evolution~~ of the flux-weighted relative RT  $\mu^*_{out}(x, t)$   
 542  $= \mathbf{n} \cdot \mathbf{Q}^*_{out}(x, t) \log_{10}(\mu_{\tau}(x, t) / \mu_{\tau}(x, 0))$  for different slopes and aquifer transmissivities.  
 543  $M^*_{out}(x, t)$  represents the difference in flux-weighted RT of the water discharged into  
 544 the river compared to the initial condition. At the start of the flood event, there is no  
 545  $\mu^*_{out}$  as river water infiltrates the aquifer. Following the decline in river stage, the aquifer  
 546 begins to discharge the mixed water with different RT back into the river (see Fig. 4c).

547

548



549



550

551 **Figure 13.** Temporal [progression evolution](#) of flux-weighted ratios of RT to the RT for  
 552 baseline conditions ( $\mu^*_{out}(x, t) = \mathbf{n} \cdot \mathbf{Q}^*_{out}(x, t) \log_{10}(\mu_t(x, t)/\mu_t(x, 0))$ ) along the river  
 553 meander as a function of  $\delta$  and  $\Gamma_d$ .  $\mu^*_{out}(x, t)$  indicates the difference of flux weighted

554 water RT (travel time) that the aquifer discharges into river compared to the initial  
 555 condition.

556

557

558 For vertical riverbank conditions ( $\delta = 90^\circ$ , top row in Fig. 13), upstream ( $0.5\lambda <$   
 559  $x < \lambda$ ) and downstream ( $0 < x < 0.5\lambda$ ) boundaries of the meander bend discharge older  
 560 and younger water, respectively. The rejuvenated or aged waters that represent shorter  
 561 and longer travel times compared to the baseline condition, respectively, were mostly  
 562 discharged before the flood event ( $t^*/t_d < 1$ ) due to the greater outflux as shown in Fig.  
 563 3a. It can also ~~can~~ be seen that water was aged along the upstream bend compared to  
 564 the more rejuvenated water along the downstream bend. After the flood event,  $\mu^*_{out}$   
 565 gradually disappears along the upstream meander (blank areas) for  $\Gamma_d = 0.1$  and 1,  
 566 because the flow fields were recovering to baseline conditions. Therefore, the upstream  
 567 meander gradually becomes the inflow boundary.

568 For cases with lower values of  $\Gamma_d$  (left columns in Fig. 13),  $\mu^*_{out}$  reaches equilibrium  
 569 earlier compared to cases with higher  $\Gamma_d$  ~~as a~~ As  $\delta$  the increasing impact of bank  
 570 slope angle causes  $\mu^*_{out}$  to gradually decrease the travel time of the outflowing water  
 571 during the flood event. For larger  $\Gamma_d$ ,  $\mu^*_{out}$  was totally dominated by rejuvenated water  
 572 during the flood event. Furthermore, ~~the stronger impact of~~ smaller bank slope angles  
 573 can both extend the time that younger water was discharging along the downstream  
 574 meander, and increase the difference in residence timesRT of these younger waters  
 575 between sloping and vertical conditions, over which and increase the magnitude with  
 576 which younger water was discharging along the downstream meander.

---

## 577 4. Discussion

### 578 4.1 Why we should account for bank slope

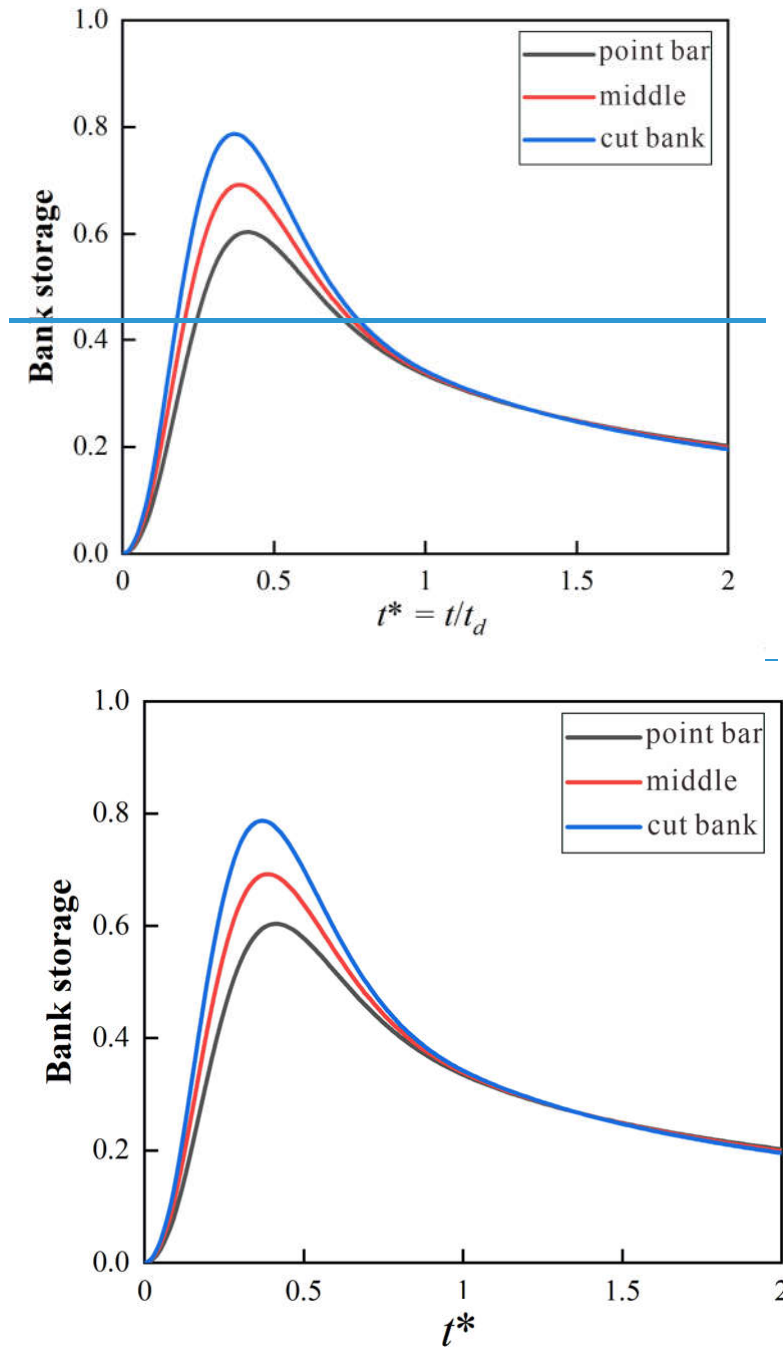
579 Tilted riverbanks are common in nature and caused by erosion and bank collapse,  
580 as has been observed at multiple scales (Zingg, 1940). Previous studies have shown that  
581 bank erosion is stronger where the river planimetry is more sinuous, river stage varies  
582 more frequently, or where the riverbank has larger sloping angles, ultimately leading to  
583 a flatter bank (Zingg, 1940; Hagorty et al., 1995; Mayor et al., 2008; Puttock et al.,  
584 2013). Yet, the impact of riverbank geometry and in particular bank slope on sinuosity-  
585 driven lateral hyporheic exchange was ignored in most previous studies. Our results  
586 clearly indicate that HZ characteristics (HEF, area and penetration distance of HZ into  
587 [the](#) alluvial valley) can be underestimated along a meandering river depending on bank  
588 slope conditions.

589 We show that not accounting for bank slope and river sinuosity can lead to an  
590 underestimation of the infiltration rate of water from the river to the alluvial aquifer (by  
591 up to 120%), as well as the area and penetration distance. This effect is more  
592 pronounced for smaller bank slope angles (Fig 5), which can be more likely found in  
593 lowland streams (Laubel et al., 2003), especially in areas with extensive cattle grazing  
594 streamside (Trimble, 1994).

595 Doble et al. (2012), Siergieiev et al. (2015) and Liang et al. (2018), assessed the  
596 influence of bank slope on HEF using a vertical cross-sectional profile. Siergieiev et al.  
597 (2015) found that the impact of bank slope on HEF was proportional to the hydraulic  
598 conductivity of the aquifer. However, we argue here that bank slope is more relevant in  
599 rivers connected to aquifers with low hydraulic transmissivity (high hydraulic  
600 conductivity or low specific yield). Furthermore, we show (Fig. 14 as example) that  
601 using only one cross-sectional river profile perpendicular to the river axis does not  
602 capture the effect of river sinuosity on HEF as bank storage decreases from point bar to

603 cut bank. This indicates that the accuracy of bank storage estimates can be improved  
 604 by including river sinuosity, which has often been omitted in the past. In a meandering  
 605 river with variable bank slope, river geometry thus has a sizable effect on bank storage  
 606 [progression evolution](#) and HEF, and should be included in any scenarios.

607



610 **Figure 14.** Bank storage versus time for  $\Gamma_d = 1$  and  $\delta = 90^\circ$  condition at: the peak of  
 611 point bar ( $x = 0$ ); middle ( $x = 0.25\lambda$ ); peak of cut bank ( $x = 0.25\lambda$ ). Dimensionless bank

612 storage was calculated by  $\frac{\int_{Y(x,t)}^{Y(x,t)+4\lambda} [h-z_b-H_0] dy}{\lambda H_p}$ .

613

## 614 **4.2 Implications of bank slope on biogeochemical reactions**

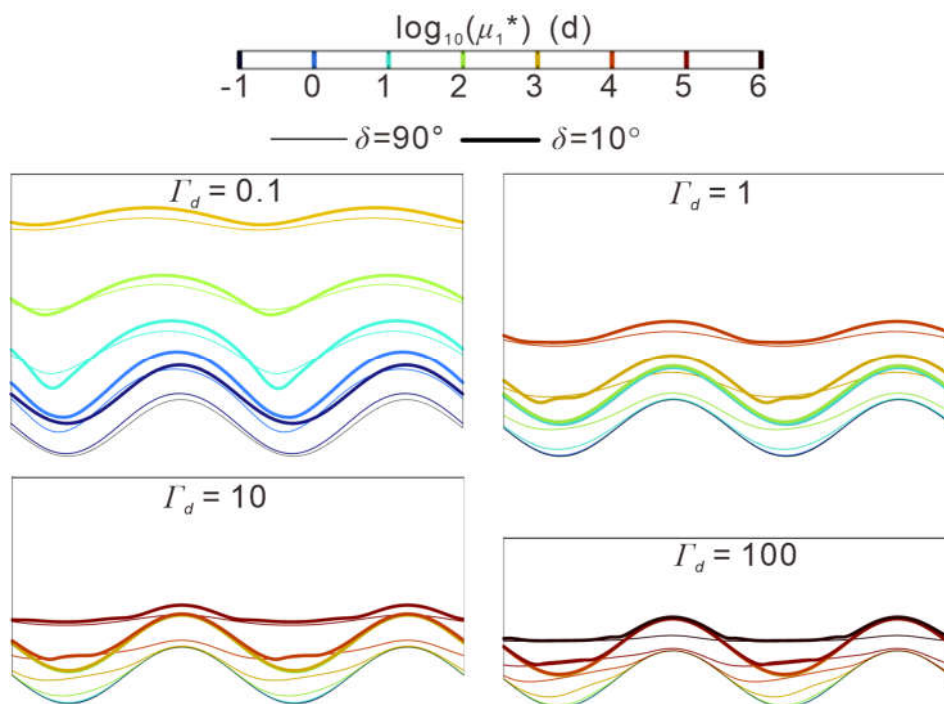
615 Under rather stable surface/surface water level  
 616 condition (base flow condition), flow conditions, the  
 617 hyporheic exchange rate and river sinuosity controls the  
 618 biogeochemical zonation (RTD) of the HZ meander  
 619 hyporheic zones. A higher hyporheic exchange rate (caused  
 620 e.g., by a whether in larger hydraulic conductivity in the  
 621 aquifer or a more sinusoidal sinuous meander) will reduce the  
 622 mean RTD and then promote promoting the biogeochemical  
 623 reactions (Boano et al., 2010; Gomez-Velez et al., 2012).  
 624 However, under for a transient flood event, the mean RTD  
 625 could be both extended and reduced dependings on the  
 626 location with respect to the meander, due to variations in the  
 627 the complex flow paths variation (Gomez-Velez et al.,  
 628 2017). Our results indicates that smaller bank slope angles  
 629 could not only increase HEF and thus lead to increased  
 630 transport of oxygen and nutrient rich stream water into the  
 631 aquifer, that bring more substances for biogeochemical  
 632 reactions in aquifer, but also alters the location and the  
 633 exposure residence time of substance this water within the  
 634 aquifer system.

635

636 Residence time distributions Mean RTDs of river water in the alluvial aquifer  
 637 have been used to evaluate the potential for biogeochemical reactions by comparing  
 638 the RT with biogeochemical timescales (BTS) for given solutes (Boano et al., 2010b;

639 Gomez-Velez et al., 2012). Locations where the ratio of RT to BTS ([terms as expressed](#)  
 640 [by Damköhler numbers](#)) is small indicate a high reaction potential for that [specific](#)  
 641 chemical species ([Gomez-Velez et al., 2015; Pinay et al., 2015](#)). It has been documented  
 642 that the BTS for dissolved organic matters (DOC) ~~is site-dependent and~~ can vary over  
 643 ten orders of magnitude ( $10^{-1} - 10^9$  d) (Hunter et al., 1998), while BTS for oxygen and  
 644 nitrate have been found to vary over eight orders of magnitude ( $10^{-2} - 10^6$  d) (Gomez-  
 645 Velez et al., 2012). Here, we compare the [mean](#) RTD within [the overlapping these two](#)  
 646 [BTS](#) ranges [of these two BTS](#) for vertical and sloping riverbank conditions ( $\delta = 10^\circ$ ) at  
 647 the peak time of the flood event ( $t^*/t_p = 0.25$ ) for different aquifer transmissivity  
 648 conditions, and show the zonation of residence times by using a BTS range of  $10^{-1} -$   
 649  $10^6$  d (Fig. 15).-

650



651

652 **Figure 15.** [Plain view of the zonation](#) of biogeochemical timescales (BTS, range of  
 653  $10^{-1} - 10^6$ ) for common HZ constituents such as DOC, oxygen or nitrate for different  
 654 aquifer transmissivities at  $t^*/t_p = 0.25$ . thick and thin lines indicate the comparison of  
 655 vertical vs sloping riverbank ( $\delta = 10^\circ$ ) conditions, while the different colors indicate the  
 656 different exponents. [Unlike the previous mean RTD figures in which the relative mean](#)



657 RTD expressed in dimensionless form, the spatial scales of mean RTD in this figure are  
 658 dimensional in days.

659

660 Fig. 15 indicates that neglecting bank slope ~~will~~impacts the prediction of reaction  
 661 potentials during ~~the~~hyporheic exchange processes, especially for locations with short  
 662 time scales. ~~For sloping bank conditions, the~~The reaction hot spots (areas , which  
 663 indicated by the overlapping BTS ranges) ~~for sloping riverbank conditions~~ expanded  
 664 further into the aquifer compared with the vertical bank conditions, ~~identical-similar~~ to  
 665 the overestimated areas in Fig. 9 to Fig. 12. Note that we did not aim to include specific  
 666 reaction models in our study but instead used mean RTD as an indicator for various  
 667 biogeochemical reactions in the aquifer. Furthermore, the wavelength of the river  
 668 sinusoid in Fig. 15 was  $\lambda = 40$  m to offer a representative riverbank-aquifer condition.  
 669 The zonation of BTSs ~~for~~ larger and smaller river sinusoid wavelengths ~~condition~~  
 670 will be reduced ~~near~~towards the river boundary or further expanded into aquifer,  
 671 respectively, for both ~~for~~ sloping and vertical riverbank conditions. Although ~~Despite~~  
 672 the dimensional BTS for various spatial scales are not shown here, ~~the~~ similar patterns  
 673 between Fig. 9-12 and Fig. 15 ~~imply~~ ~~have proven the implication~~ the usability of the  
 674 mean RTD results (Fig. 9-12) ~~regard to~~ ~~infer on~~ potential biogeochemical reactions.

675 The ~~Impact~~impact of bank slope on RT is basically controlled by aquifer  
 676 transmissivity. ~~When~~For higher aquifer transmissivity conditions ~~increases~~ ~~aquifer~~, the  
 677 impact of bank slope appears to be more pronounced when the river stage rises during  
 678 a flood event. For ~~decreasing~~lower aquifer transmissivity aquifer conditions, bank  
 679 slope seems more relevant for mean RTD after the flood event and its impact is more  
 680 long-lasting. Smaller ~~b~~Bank slope angles could ~~result in longer~~ ~~extend~~ (near the point  
 681 bar) or ~~shorter~~ ~~reduce~~ (near the cut bank) pore water travel times throughout the flood  
 682 event, compared to the non-sloping (vertical) riverbank condition. This ~~means~~  
 683 indicates that compared with the vertical riverbank condition, point bars with bank  
 684 slopes are more favorable for removing dissolved organic carbon and for nitrification,

685 while cut banks with bank slope may have adverse effects on the groundwater quality  
686 near rivers. [The vertical profile modelling study of Derx et al. \(2014\)](#) suggested for ~~that~~  
687 ~~the bank-riverbank restoration projects, –which-increasing~~ HEF by reducing the slope  
688 ~~angle may have a negative effect on restoration.~~ The mean RTD results of this study  
689 ~~also suggest that the role of the impact of bank slope on groundwater quality is~~  
690 ~~determined by the location with respect to the meander (near point bar or cut bank).~~ As  
691 such, ~~an-our~~ analysis of ~~residence time distributions~~ [mean RTDs](#) can provide valuable  
692 information on whether and where riverbank slope can induce biogeochemical hotspots  
693 and hot moments and help guide choices to be made in biogeochemical field surveys  
694 regarding location and sampling time under dynamic river stage conditions, especially  
695 when the connected aquifers have low hydraulic transmissivity.

696

### 697 **4.3 Advantages and limitations of using a reduced 2-D model**

698 In this study, we propose a parsimonious reduced-order, idealized horizontal 2-D  
699 model that simplifies the variation of the river-aquifer interface by using the moving  
700 boundary method to depict the displacement of the SWI along a sloping riverbank. An  
701 advantage of this approach is reduced model complexity as compared to a three-  
702 dimensional model, which greatly reduces time and data requirements during model  
703 building and computational demand during the simulation of HEF and especially  
704 residence time distributions. Thus, our reduced-order model acts as a first step to gain  
705 insight into the patterns of hyporheic exchange, riverbank storage and [mean](#) RTD in  
706 settings with more complex riverbank morphology and dynamic forcing. Future efforts  
707 should be focused on optimizing the computational method applied here and on  
708 including more detailed morphology and hydrodynamic characteristics.

709 In our simulations we assume a constant bank slope angle along the entire  
710 meandering river while natural riverbanks often change their slope angle from reach to  
711 reach as well as with time. This variability could lead to more complex SWI travel

---

712 distances and residence time distributions, and new conceptualizations that account for  
713 the contribution of bank slope on time-varying RTD and HZ extent are needed. In our  
714 simulations we tested the model using a range of aquifer hydraulic conductivities.  
715 Although hydraulic conductivity (or transmissivity) is a critical parameter in the  
716 quantification of exchange fluxes and RTD between the two systems under varying  
717 slope conditions, other parameters such as valley water head fluctuation, water  
718 abstraction e.g. for agriculture or drinking water supply, peak flood event characteristics  
719 or larger scale groundwater head fluctuation, e.g., due to changing groundwater  
720 recharge in the context of changing rainfall patterns have not been considered here but  
721 might also impact HZ extent, RTD and river-aquifer exchange flux. For example, valley  
722 water head fluctuation and water abstraction in the aquifer will lead to a lower  
723 groundwater table, increasing the hydraulic gradient between river and aquifer. This  
724 will lead to the formation of a larger HZ area as well as longer travel distances and  
725 times of river water in the aquifer. Thus, reducing the slope of the river bank could  
726 reduce the infiltration of polluted river water into the riparian aquifer.

727       The current study assumes a perennial stream and unconfined (phreatic) conditions  
728 in the connected aquifer as well as changing hydraulic gradients leading to gaining and  
729 losing conditions in the river. Where there is no hydraulic gradient between river and  
730 aquifer, no large-scale infiltration of river water into the riverbanks will occur, while  
731 local turbulent flow (e.g., due to obstacles in the river channel) might lead to localized  
732 infiltration over short distances and short time scales (Sawyer et. al., 2011; Stonedahl  
733 et al., 2013; Käser et al., 2013). Where the unconfined layer is small (e.g., in  
734 mountainous headwater streams with a rather small sediment layer overlying a hard-  
735 rock aquifer with relatively low hydraulic conductivity), the HZ is limited in its  
736 maximum extent, and travel times and distances are considerably shorter. However, in  
737 mountainous settings, slope angles are often much steeper due to erosion (here rivers  
738 incising into the bedrock) and further simulations are required to better understand the  
739 feedback between banks slope angle, hydraulic gradient and maximum extent of the

740 unconfined layer allowing for ~~hyporheic exchange processes~~ ~~reasonable river water~~  
741 ~~infiltration~~. These simulations will also help us better understand the impact of bank  
742 slope on ~~quantitative and qualitative~~ water supply ~~to abstraction wells~~ ~~and water quality~~  
743 ~~to abstraction wells~~, e.g., used for the production of drinking water.

744 While ~~the~~ using the Boussinesq equation neglects the influence of the vadose zone,  
745 this approach as well as the assumption of ~~a~~ vertically integrated distribution of  
746 hydraulic head have been widely used in the literature and proven adequate when  
747 simulating sinuosity-driven HEF patterns (Boano et al., 2006; 2010., Cardenas. 2008;  
748 2009a, b; Gomez-Velez et al., 2012; 2017, Kruegler et al., 2020). While we found  
749 differences in HEF patterns when comparing simple models using the Boussinesq with  
750 those using Richard's equation (S4 in SI) these differences exist independent of using  
751 the DGM. However, we recommend in future studies to more systematically consider  
752 these two different approaches with respect to their advantages and limitations, e.g., in  
753 terms of computability or efficiency in predicting HEF under various conditions. While  
754 in an ideal scenario a 3-D modeling approach includes vadose zone and riverbank slope  
755 angle (both variable in time and space), for the moment the implementation of such  
756 detailed models in practice suffers from limited computing capabilities.

## 757 5. Conclusions

758 The deformed geometry method was applied to characterize the expansion and  
759 contraction of hyporheic zones along sloping riverbanks, and to evaluate the impact of  
760 bank slope on hyporheic exchange flux, ~~progression evolution~~ of the HZ area and  
761 residence (travel) time distributions of the infiltrating water. To achieve this, several  
762 unconfined alluvial aquifers with varying slope angles and aquifer transmissivity values  
763 were simulated. Our results show that bank slope in a sinuosity-driven river was non-  
764 negligible when the aims of numerical/analytical models are the prediction of the  
765 ~~progression evolution~~ of the hyporheic zone during and after a flood event (transient

---

766 flood forcing).

767 The overall findings of our work underline the need for including more realistic  
768 riverbank morphological conditions into simulations when studying lateral hyporheic  
769 exchange flow responses to dynamic forcings. Furthermore, our results show that more  
770 detailed information on bank slope (e.g., through more measurements) can lead to a  
771 better understanding of hyporheic flow patterns and potentially result in improved  
772 biochemical process understanding for real-world conditions for more complex  
773 morphological and depositional environments. Several conclusions can be drawn from  
774 our study:

- 775 1. Sloping riverbanks can considerably increase HEF during a flood event, especially  
776 when the river is connected to an alluvial aquifer with rather high hydraulic  
777 conductivity and small bank slope angles as water can more easily infiltrate the  
778 connected aquifer. Smaller bank slope angles can lead to an extended hyporheic  
779 zone with river water infiltrating deeper (penetration distance) into the aquifer.  
780 However, bank slope has only a minor impact on the hyporheic outflow flux (water  
781 re-entering the stream).
- 782 2. During a flood event, the impact of bank slope on [mean](#) residence time distributions  
783 (RTD) is more pronounced for [aquifers with high hydraulic transmissivity](#) ~~aquifers~~,  
784 due to the larger area and deeper penetration distance of the HZ for these conditions.  
785 On the contrary, the impact of bank slope on [mean](#) RTD for lower transmissivity  
786 aquifers is minor during the flood event, but bank slope can have a significant and  
787 long-lasting effect ~~for post-flood conditions~~.
- 788 3. River sinuosity should be considered when assessing the impact of bank slope on  
789 [mean](#) RTD. Variable bank slope can lead to both longer and shorter residence times  
790 when compared to vertical riverbank conditions.
- 791 4. Bank slope has a greater impact on the residence time of hyporheic water in lower-  
792 transmissivity aquifers, thereby delaying the time of younger water discharge  
793 downstream of a meander bend, which also delays the outflow of older water

---

794

upstream of that bend.

795 **Code and data availability**

796 Additional information regarding methodology and results is provided in the supporting  
797 information (SI).

798 **Author contributions**

799 YL: Conceptualization, Formal analysis, Methodology, Investigation, Writing

800 US: Conceptualization, Methodology, Writing

801 ZW: Funding acquisition, Software, Supervision

802 SK: Validation, Writing, Supervision

803 HL: Project administration, Supervision

804 **Acknowledgements**

805 This research was partially supported by the National Natural Science Foundation of  
806 China (Grant Numbers: 42272290, 41830862, and 42022018), and China Scholarship  
807 Council (CSC, 202106410042). [Funding from the Royal Society \(INF\R2\212060\) for  
808 S.K. and the Leverhulme Trust \(RPG-2021-030\) for S.K. and U.S is also acknowledged.](#)

809

810 **Competing interests**

811 The authors declare that they have no conflict of interest.

---

**812 References**

- 813 Bear, J., and Cheng, A. H. D.: Modeling groundwater flow and contaminant transport,  
814 Vol. 23, pp. 83, Dordrecht: Springer, 2010.
- 815 Bertrand, G., Goldscheider, N., Gobat, J.-M., and Hunkeler, D.: Review: From multi-  
816 scale conceptualization to a classification system for inland groundwater-  
817 dependent ecosystems, *Hydrogeology Journal*, 20, 5-25, 2012.
- 818 Boano, F., Camporeale, C., Revelli, R., and Ridolfi, L.: Sinuosity-driven hyporheic  
819 exchange in meandering rivers, *Geophysical Research Letters*, 33, L18406, 2006.
- 820 Boano, F., Harvey, J. W., Marion, A., and Packman, A. I., Revelli, R., Ridolfi, L., and  
821 Wörman, A.: Hyporheic flow and transport processes: Mechanisms, models, and  
822 biogeochemical implications, *Reviews of Geophysics*, 52, 603-679, 2014.
- 823 Boano, F., Demaria, A., Revelli, R., and Ridolfi, L.: Biogeochemical zonation due to  
824 intrameander hyporheic flow, *Water Resource. Research.* 46, W02511, 2010.
- 825 Boano, F., Revelli, R., and Ridolfi, L.: Effect of streamflow stochasticity on bedform-  
826 driven hyporheic exchange. *Advances in Water Resources*, 33(11), 1367-1374.  
827 2010. Boulton, A. J., Datry, T., Kasahara, T., Mutz, M., and Stanford, J. A.: Ecology  
828 and management of the hyporheic zone: Stream-groundwater interactions of  
829 running waters and their floodplains, *Journal of the North American Benthological*  
830 *Society*, 29 (1), 26-40, 2010.
- 831 Brunke, M., and Gonser, T.: The ecological significance of exchange processes between  
832 rivers and groundwater, *Freshwater Biology*, 37 (1), 1-33, 1997.
- 833 Cardenas, M. B.: The effect of river bend morphology on flow and timescales of surface  
834 water-groundwater exchange across pointbars, *Journal of Hydrology*, 362, 134-  
835 141, 2008.
- 836 Cardenas, M. B.: A model for lateral hyporheic flow based on valley slope and channel  
837 sinuosity, *Water Resources Research*, 45, W01501, 2009a.
- 838 Cardenas, M. B.: Stream-aquifer interactions and hyporheic exchange in gaining and



- 
- 839        losing sinuous streams, *Water Resources Research*, 45, W06429, 2009b.
- 840        Cardenas, M. B.: Hyporheic zone hydrologic science: A historical account of its  
841        emergence and a prospectus, *Water Resources Research*, 51, 3601-3616, 2015.
- 842        [COMSOL Multiphysics. Introduction to COMSOL multiphysics. Version 5.5.](#)  
843        [COMSOL. Burlington, MA. 2019.](#)
- 844        Cooper, H. H., and Rorabaugh, M. I.: Ground-water movements and bank storage due  
845        to flood stages in surface streams, Report of Geological Survey Water-Supply, pp.  
846        1536-J, US Government Printing Office, Washington, United States, 1963.
- 847        Derx, J., Farnleitner, A. H., Blöschl, G., Vierheilig, J., and Blaschke, A. P.: Effects of  
848        riverbank restoration on the removal of dissolved organic carbon by soil passage  
849        during floods—A scenario analysis, *Journal of Hydrology*, 512, 195-205, 2014.
- 850        Doble, R. C., Crosbie, R. S., Smerdon, B. D., Peeters, L., and Cook, F. J.: Groundwater  
851        recharge from overbank floods, *Water Resources Research*, 48 (9), W09522,  
852        2012a.
- 853        Doble, R., Brunner, P., McCallum, J., and Cook, P. G.: An analysis of river bank slope  
854        and unsaturated flow effects on bank storage, *Ground Water*, 50 (1), 77-86, 2012b.
- 855        Donea, J., A. Huerta, J.-P. Ponthot, and A. Rodriguez-Ferran.: Arbitrary Lagrangian–  
856        Eulerian methods, In *Encyclopedia of Computational Mechanics*, ed. E. Stein, R.  
857        de Borst, and T. J. R. Hughes, 413-434. New York: John Wiley & Sons, 2004.
- 858        Duarte, F., Gormaz, R., and Natesan, S.: Arbitrary Lagrangian–Eulerian method for  
859        Navier–Stokes equations with moving boundaries, *Computer Methods in Applied*  
860        *Mechanics and Engineering*, 193 (45-47), 4819-4836, 2004.
- 861        Fox, G. A., and Wilson, G. V.: The role of subsurface flow in hillslope and stream bank  
862        erosion: a review, *Soil Science Society of America Journal*, 74 (3), 717-733, 2010.
- 863        Gao, Y., Zhu, B., Zhou, P., Tang, J. L., Wang, T., and Miao, C. Y.: Effects of vegetation  
864        cover on phosphorus loss from a hillslope cropland of purple soil under simulated  
865        rainfall: a case study in China, *Nutrient Cycling in Agroecosystems*, 85 (3), 263-  
866        273, 2009.

- 
- 867 Gomez-Velez, J. D., and Harvey, J. W.: A hydrogeomorphic river network model  
868 predicts where and why hyporheic exchange is important in large basins,  
869 Geophysical Research Letters, 41, 6403–6412, 2014.
- 870 Gomez-Velez, J. D., Wilson, J. L., and Cardenas, M. B.: Residence time distributions  
871 in sinuosity-driven hyporheic zones and their biogeochemical effects, Water  
872 Resources Research, 48 (9), 2012.
- 873 Gomez-Velez, J. D., Wilson, J. L., Cardenas, M. B., and Harvey, J. W.: Flow and  
874 residence times of dynamic river bank storage and sinuosity-driven hyporheic  
875 exchange, Water Resources Research, 53, 8572-8595, 2017.
- 876 Gomez-Velez, J. D., Harvey, J. W., Cardenas, M. B., and Kiel, B.: Denitrification in the  
877 Mississippi River network controlled by flow through river bedforms, Nature  
878 Geoscience, 8, 941-945, 2015.
- 879 Hagerty, D. J., Spoor, M. F., and Parola, A. C.: Near-bank impacts of river stage control,  
880 Journal of Hydraulic Engineering, 121 (2), 196-207, 1995.
- 881 Hooke, J. M.: River meandering, In E. Wohl & J. Shroder (Eds.), Treatise on  
882 geomorphology, Vol. 9, pp. 260-288, CA: Academic Press, San Diego, 2013.
- 883 Hester, E. T., and Gooseff, M. N.: Moving beyond the banks: Hyporheic restoration is  
884 fundamental to restoring ecological services and functions of streams,  
885 Environmental Science and Technology, 44 (5), 1521-1525, 2010.
- 886 Hunt, B.: An approximation for the bank storage effect, Water Resources Research, 26  
887 (11), 2769–2775, 1990.
- 888 Hunter, K. S., Wang, Y., Van, C. P.: Kinetic modeling of microbially-driven redox  
889 chemistry of subsurface environments: coupling transport, microbial metabolism  
890 and geochemistry. Journal of hydrology, 209 (1-4), 53-80, 1998.
- 891 Käser, D. H., Binley, A., and Heathwaite, A. L.: On the importance of considering  
892 channel microforms in groundwater models of hyporheic exchange. River  
893 Research and Applications, 29(4), 528-535, 2013.
- 894 Kiel, B. A., Cardenas, M. B.: Lateral hyporheic exchange throughout the Mississippi

- 
- 895 River network, *Nature Geoscience*, 7 (6), 413-417, 2014.
- 896 Krause, S., Abbott, B. W., Baranov, V., Bernal, S., Blaen, P., Datry, T., Drummond, J.,  
897 Fleckenstein, J. H., Gomez-Velez, J., Hannah, D. M., Knapp, J. L. A., Kurz, M.,  
898 Lewandowski, J., Marti, E., Mendoza-Lera C., Milner, A., Packman, A., Pinay, G.,  
899 Ward, A. S., Zarnetzke, J. P.: Organizational principles of hyporheic exchange flow  
900 and biogeochemical cycling in river networks across scales, *Water Resources*  
901 *Research*. 58, e2021WR029771, 2022.
- 902 Krause, S., Hannah, D. M., Fleckenstein, J. H., Heppell, C. M., Pickup, R., Pinay, G.,  
903 Robertson, A. L., and Wood, P. J.: Inter-disciplinary perspectives on processes in  
904 the hyporheic zone, *Ecohydrology Journal*. 4 (4), 481-499, 2011.
- 905 Krause, S., Lewandowski, J., Grimm, N., Hannah, D. M., Pinay, G., Turk, V., Argerich,  
906 A., Sabater, F., Fleckenstein, J., Schmidt, C., Battin, T., Pfister, L., Martí, E.,  
907 Sorolla, A., Larned, S., and Turk, V.: Ecohydrological interfaces as critical  
908 hotspots for ecosystem functioning, *Water Resources Research*. 53, 6359-6376,  
909 2017.
- 910 Krause, S., Tecklenburg, C., Munz, M., and Naden, E.: Streambed nitrogen cycling  
911 beyond the hyporheic zone: Flow controls on horizontal patterns and depth  
912 distribution of nitrate and dissolved oxygen in the upwelling groundwater of a  
913 lowland river, *Journal of Geophysical Research: Biogeosciences*, 118 (1), 54-67,  
914 2013.
- 915 Kruegler, J., Gomez-Velez, J. D., Lautz, L. K., and Endreny, T. A.: Dynamic  
916 evapotranspiration alters hyporheic flow and residence times in the intrameander  
917 zone, *Water*, 12 (2), 424, 2020.
- 918 Larkin, R. G., and Sharp, J. M.: On the relationship between river-basin geomorphology,  
919 aquifer hydraulics, and groundwater flow direction in alluvial aquifers, *Geological*  
920 *Society of America Bulletin*, 104, 1608-1620, 1992.
- 921 Laubel, A., Kronvang, B., Hald, A. B., and Jensen, C.: Hydromorphological and  
922 biological factors influencing sediment and phosphorus loss via bank erosion in

- 
- 923 small lowland rural streams in Denmark. *Hydrological processes*, 17(17), 3443-  
924 3463, 2003.
- 925 Li, H., Boufadel, M. C., and Weaver, J. W.: Quantifying bank storage of variably  
926 saturated aquifers, *Ground Water*, 46 (6), 841-850, 2008.
- 927 Liang, X. Y., Zhan, H. B., and Schilling, K.: Spatiotemporal responses of groundwater  
928 flow and aquifer-river exchanges to flood events, *Water Resources Research*, 54  
929 (3), 1513-1532, 2018.
- 930 Lindow, N., Fox, G. A., and Evans, R. O.: Seepage erosion in layered stream bank  
931 material, *Earth Surface Processes and Landforms*, 34 (12), 1693-1701, 2009.
- 932 Mayor, Á. G., Bautista, S., Small, E. E., Dixon, M., and Bellot, J.: Measurement of the  
933 connectivity of runoff source areas as determined by vegetation pattern and  
934 topography: A tool for assessing potential water and soil losses in drylands, *Water  
935 Resources Research*, 44 (10), 2008.
- 936 Maury, B.: Characteristics ALE method for the unsteady 3D Navier-Stokes equations  
937 with a free surface, *International Journal of Computational Fluid Dynamics*, 6 (3),  
938 175-188, 1996.
- 939 McCallum, J.L., P.G. Cook, P. Brunner, and D, Berhane.: Solute dynamics during bank  
940 storage flows and implications for chemical baseflow separation, *Water Resources  
941 Research*, 46: W07541, 2010.
- 942 McClain, M. E., Boyer, E. W., Dent, C. L., Gergel, S. E., Grimm, N. B., Groffman, P.  
943 M., Hart, S. C., Harvey, J. W., Johnston, C. A., Mayorga, E., Mcdowell, W and  
944 Pinay, G.: Biogeochemical hot spots and hot moments at the interface of terrestrial  
945 and aquatic ecosystems, *Ecosystems*, 6 (4), 301-312, 2003.
- 946 Millar, R. G., and Quick, M. C.: Effect of bank stability on geometry of gravel rivers,  
947 *Journal of Hydraulic Engineering*, 119 (12), 1343-1363, 1993.
- 948 Millington, R. J., and Quirk, J. P.: Permeability of porous solids, *Transactions of the  
949 Faraday Society*, 57, 1200-1207, 1961.
- 950 Osman, A. M., and Thorne, C. R.: Riverbank stability analysis. I: Theory, *Journal of*

- 
- 951 Hydraulic Engineering, 114 (2), 134-150, 1988.
- 952 Pinay, G., Peiffer, S., De Dreuzy, J. R., Krause, S., Hannah, D. M., Fleckenstein, J. H.,  
953 Sebilo, M., Bishop, K., and Hubert-M, L.: Upscaling nitrogen removal capacity  
954 from local hotspots to low stream orders' drainage basins, *Ecosystems*, 18 (6),  
955 1101-1120, 2015.
- 956 Pohjoranta, A., and Tenno, R.: Implementing surfactant mass balance in 2D FEM–ALE  
957 models, *Engineering with Computers*, 27 (2), 165-175, 2011.
- 958 Puttock, A., Macleod, C. J., Bol, R., Sessford, P., Dungait, J., and Brazier, R. E.:  
959 Changes in ecosystem structure, function and hydrological connectivity control  
960 water, soil and carbon losses in semi-arid grass to woody vegetation transitions,  
961 *Earth Surface Processes and Landforms*, 38 (13), 1602-1611, 2013.
- 962 Seminara, G.: Meanders, *Journal of Fluid Mechanics*, 554, 271-297, 2006.
- 963 Schmadel, N. M., A. S. Ward, C. S. Lowry, and J. M. Malzone.: Hyporheic exchange  
964 controlled by dynamic hydrologic boundary conditions, *Geophysical Research*  
965 *Letters*, 43, 4408-4417, 2016.
- 966 Sawyer, A. H., Bayani Cardenas, M., and Buttle, J.: Hyporheic exchange due to  
967 channel-spanning logs. *Water Resources Research*, 47(8), 2011.
- 968 Sharp, J. M.: Limitations of bank-stoppage model assumptions, *Journal of Hydrology*,  
969 35 (1-2), 31-47, 1977.
- 970 Siergieiev, D., Ehlert, L., Reimann, T., Lundberg, A., and Liedl, R.: Modelling  
971 hyporheic processes for regulated rivers under transient hydrological and  
972 hydrogeological conditions, *Hydrology and Earth System Sciences*, 19 (1), 329-  
973 340, 2015.
- 974 Singh, T., Gomez-Velez, J. D., Wu, L., Wörman, A., Hannah, D. M., and Krause, S.:  
975 Effects of successive peak flow events on hyporheic exchange and residence times,  
976 *Water Resources Research*, 56 (8), e2020WR027113, 2020.
- 977 Singh, T., Wu, L., Gomez-Velez, J. D., Lewandowski, J., Hannah, D. M., Krause, S.:  
978 Dynamic hyporheic zones: Exploring the role of peak flow events on bedform-

- 
- 979 induced hyporheic exchange, *Water Resources Research*, 55, 218-235, 2019.
- 980 Stonedahl, S. H., Harvey, J. W., and Packman, A. I.: Interactions between hyporheic  
981 flow produced by stream meanders, bars, and dunes, *Water Resources Research*,  
982 49, 5450-5461, 2013.
- 983 Trimble, S. W.: Erosional effects of cattle on streambanks in Tennessee, USA. *Earth*  
984 *surface processes and landforms*, 19(5), 451-464, 1994.
- 985 Triska, F. J., Kennedy, V. C., Avanzino, R. J., Zellweger, G. W., and Bencala, K. E.:  
986 Retention and transport of nutrients in a third - order stream in northwestern  
987 California: Hyporheic processes, *Ecology*, 70 (6), 1893-1905, 1989.
- 988 Van Genuchten, M. T.: A closed - form equation for predicting the hydraulic  
989 conductivity of unsaturated soils. *Soil science society of America journal*, 44(5),  
990 892-898, 1980.
- 991 Weatherill, J. J., Atashgahi, S., Schneidewind, U., Krause, S., Ullah, S., Cassidy, N.,  
992 and Rivett, M. O.: Natural attenuation of chlorinated ethenes in hyporheic zones:  
993 A review of key biogeochemical processes and in-situ transformation potential,  
994 *Water research*, 128, 362-382, 2018.
- 995 Wondzell, S. M., and Swanson, F. J.: Floods, channel change, and the hyporheic zone,  
996 *Water Resources Research*, 35 (2), 555-567, 1999.
- 997 Wu, L., Gomez-Velez, J. D., Krause, S., Singh, T., Wörman, A., and Lewandowski, J.:  
998 Impact of flow alteration and temperature variability on hyporheic exchange,  
999 *Water Resources Research*, 56 (3), e2019WR026225, 2020.
- 1000 Wu, L., Gomez-Velez, J. D., Krause, S., Wörman, A., Singh, T., Nützmann, G., and  
1001 Lewandowski, J.: How daily groundwater table drawdown affects the diel rhythm  
1002 of hyporheic exchange, *Hydrology and Earth System Sciences*, 25 (4), 1905-1921,  
1003 2021.
- 1004 Wu, L., Singh, T., Gomez-Velez, J. D., Nützmann, G., Wörman, A., Krause, S., and  
1005 Lewandowski, J.: Impact of dynamically changing discharge on hyporheic  
1006 exchange processes under gaining and losing groundwater conditions, *Water*

- 
- 1007 Resources Research, 54 (12), 10-076, 2018.
- 1008 Zarnetske, J. P., Haggerty, R., Wondzell, S. M., and Baker, M. A.: Dynamics of nitrate  
1009 production and removal as a function of residence time in the hyporheic zone,  
1010 Journal of Geophysical Research, 116, G01025, 2021.
- 1011 Zarnetske, J. P., Haggerty, R., Wondzell, S. M., Bokil, V. A., and González-Pinzón, R.:  
1012 Coupled transport and reaction kinetics control the nitrate source-sink function of  
1013 hyporheic zones, Water Resources Research, 48, W11508, 2012.
- 1014 Zingg, A. W.: Degree and length of land slope as it affects soil loss in run-off,  
1015 Agricultural Engineering, 21, 59-64, 1940.
- 1016